

---

# MINDSET: VISION. A TOOLBOX FOR TESTING DNNs ON KEY PSYCHOLOGICAL EXPERIMENTS

---

A PREPRINT

Valerio Biscione<sup>1\*</sup> Milton L. Montero<sup>3\*</sup> Marin Dujmovic<sup>2\*</sup>  
Gaurav Malhotra<sup>4</sup> Dong Yin<sup>5</sup> Guillermo Puebla<sup>6</sup> Federico Adolfi<sup>2,7</sup>  
Rachel F. Heaton<sup>8</sup> John E. Hummel<sup>8</sup> Benjamin D. Evans<sup>9</sup> Karim Habashy<sup>2</sup>  
Jeffrey S. Bowers<sup>2</sup>

<sup>1</sup>Independent; <sup>2</sup> University of Bristol; <sup>3</sup>IT University of Copenhagen; <sup>4</sup>SUNY Albany  
<sup>5</sup>Cambridge University; <sup>6</sup>Universidad de Tarapacá; <sup>7</sup>Ernst Strüngmann Institute for Neuroscience  
<sup>8</sup> University of Illinois Urbana-Champaign; <sup>9</sup> University of Sussex

valerio.biscione@gmail.com; mlle@itu.dk {marin.dujmovic,j.bowers}@bristol.ac.uk

March 27, 2026

## ABSTRACT

Multiple benchmarks have been developed to assess the alignment between deep neural networks (DNNs) and human vision. In almost all cases these benchmarks are observational in the sense they are composed of behavioural and brain responses to naturalistic images that have not been manipulated to test hypotheses regarding how DNNs or humans perceive and identify objects. Here we introduce the toolbox *MindSet: Vision*, consisting of a collection of image datasets and related scripts designed to test DNNs on 30 psychological findings. In all experimental conditions, the stimuli are systematically manipulated to test specific hypotheses regarding human visual perception and object recognition. In addition to providing pre-generated datasets of images, we provide code to regenerate these datasets, offering many configurable parameters which greatly extend the dataset versatility for different research contexts, and code to facilitate the testing of DNNs on these image datasets using three different methods (similarity judgments, out-of-distribution classification, and decoder method), accessible via GitHub. To illustrate the challenges these datasets pose for developing better DNN models of human vision, we test several models on range of datasets included in the toolbox.

## 1 Introduction

Deep neural networks (DNNs) provide the best engineering solution to identifying objects short of biological vision, and many researchers claim that DNNs are the best current models of human vision and object recognition [1–5]. Key evidence in support of this claim comes from the finding that DNNs perform the best on various behavioural and brain benchmarks. In the case of behavioural benchmarks, models are assessed on how well they account for human (or macaque) errors in classifying a large set of objects [6–8], or how well they predict human similarity judgements [9, 10]. In the case of brain benchmarks, models are assessed with regard to how well they predict brain recordings (e.g., single-cell responses or fMRI data) in response to a set of objects [8, 11–13]. The general assumption is that the better a model does at predicting the data, the more similar the model is to biological vision. For instance, the Brain-Score benchmark is described as “a composite of multiple neural and behavioural benchmarks that score any [artificial neural network] on how similar it is to the brain’s mechanisms for core object recognition” [11]

A common feature of most benchmark studies is that they treat the to-be-predicted data as observational. That is, there is rarely an attempt to predict the impact of experimental manipulation designed to test specific hypotheses about how

---

\*equal contribution

human or machine vision works. Rather, observers perform a single task over a set of images that satisfies some general criterion, such as objects presented in isolation [14], in naturalistic contexts [8–10, 13], or on a range of arbitrary backgrounds [11, 15]. This approach is problematic because it is possible to make good predictions on these datasets even when models identify objects in qualitatively different ways than monkeys or humans [16]. This is possible whenever images contain multiple diagnostic cues for object classification. For example, a DNN that classifies objects by texture might still be able to predict brain activation in a visual system that classifies objects by shape because the texture and shape of objects are confounded. Indeed, multiple confounds may drive predictions. For example, Malhotra and Bowers [17] showed that the Brain-Score predictions of visual regions V4 and IT are largely driven by the scene backgrounds rather than the objects themselves.

The standard way to rule out confounds in order to determine causal relations (e.g. inferring that DNNs learn brain-like representations) is to carry out experiments designed to rule out confounds as the basis of making good predictions. In fact, there is a large literature in psychology describing experiments designed to test specific hypotheses about how human vision works, but surprisingly, this literature is often ignored when modellers compare DNNs to biological vision (for notable exceptions see the review paper [18]). [19] reviewed a wide range of psychological phenomena that current DNNs either fail to capture or that have yet to be considered. Furthermore, when researchers do consider the psychological literature when making claims regarding DNN-human similarities, the models are rarely subject to the kind of “severe” tests that are required to make any strong conclusions, that is tests that are likely to challenge claims in case they are false. Instead, strong conclusions are often drawn based on superficial similarities [20].

There are at least four (related) reasons for this current state of affairs. First, many researchers in computer science and computational neuroscience may be unfamiliar with the rich set of experiments carried out in psychology that manipulate independent variables to better understand human vision, memory, language, etc. Those who are aware of these studies might find it challenging to engage with them, as psychological datasets are not readily available in formats that the community is accustomed to working with. Second, it is not always obvious how one should test a model against psychological data. Hence, it may be easier to focus on improving performance on the current benchmarks, and this may have discouraged researchers from exploring data from psychology. A third potential reason is an overall skepticism towards psychological results, a sentiment that may reflect the well-documented replication crisis in psychology [21]. Forth, there is a strong bias to look for DNN-human similarities and downplay the differences [20], and severely testing on psychological data might not result in similarities. However, characterizing these failures provides key insights into the ways DNNs need to be improved when modelling biological vision.

Here we present *MindSet: Vision*, a toolbox aimed at facilitating testing DNNs on visual psychological phenomena by addressing all the problems presented above: our main contribution is to provide a large, easily accessible, parameterized, set of 30 image datasets (and related scripts to re-generate and modify them) accounting for a wide array of well-replicated visual experiment and phenomena reported in psychology. Our stimuli cover aspects of low and mid-level vision (including Gestalt phenomena), visual illusions, and object recognition tasks. While our stimuli primarily focus on static vision, reflecting the current emphasis in DNN/human alignment research, we recognize the importance of other areas of vision, such as dynamic processes like motion perception. We hope that our work serves as a solid foundation for further investigation into these complex cognitive processes. We provide a high-level descriptions of the visual phenomena in the main text (Section 2) and more detailed descriptions in the Appendix (A).

To facilitate experimentation across a variety of scenarios, each dataset can be easily regenerated across different configurations (image size, background colour, stroke colour, number of samples, etc.). To address the difficulty in testing DNNs on these stimuli, we provide scripts for using one (or more) of three methods: Similarity Judgment Analysis, Decoder Approach, and Out-of-Distribution classification (Section 3) and an extensively documented code (Section 6). Importantly, we also highlight how these analysis methods and datasets can be used to characterize DNN-brain alignment by testing 15 DNNs on a set of 9 of the experiments included in the toolkit. These experiments are not intended to provide a strong test of how well these DNNs model biological vision. But they do demonstrate new challenges of modeling biological vision, and the importance of considering psychological experiments when building models of human vision.

With *MindSet: Vision*, we aim to bridge the gap between computational modeling and psychological research, bringing experimental studies that manipulate independent variables to the forefront of developing and evaluating of DNN models of human vision. We also hope this initiative will drive further interest in other areas of human psychology, such as memory, language, and speech perception when attempting to understand and replicate human-like intelligence in machines.

## 1.1 Related Work

Several recent studies share some similarities with our project: [22] propose a human-validated dataset of five types of brightness illusions and benchmark three DNNs on their ability to identify and localize these illusions. [23] introduced a new dataset containing five types of visual illusions falling into two categories: color constancy and geometrical illusions. The authors formulated four tasks specifically designed to examine the performance of Visual Language Models, finding low alignment with human responses. [24] developed the Good Gestalt datasets, consisting of six types of datasets covering several types of Gestalt grouping principles, including Closure, Continuity, and Proximity, aimed at testing a Latent Noise Segmentation Network. Similarly, [25] developed the model-vs-human benchmark that compares ANN-human classification errors on various ‘out-of-distribution’ datasets composed of naturalistic images that were modified in various ways, including low-level feature manipulations of contrast and spatial frequency, as well as higher-level manipulations, such as generating silhouettes and sketches of images. More recently, the Brain-Score benchmark has included several behavioural and brain benchmark studies composed of stimuli taken from psychological experiments, including three experiments included in the MindSet Vision: toolkit (See the Baker2022 and BMD2024 datasets at <https://www.brain-score.org/vision/>). In comparison to these works, we present a toolbox to test DNNs on a much wider range of visual psychological effects and provide the code base to regenerate images in batches, changing the parameters, and testing each one of them on a variety of methods. This facilitates the systematic and severe testing of models on each of the 30 experiments in the toolbox.

## 2 Datasets

We have included datasets from experiments that characterize a wide range of visual phenomena, ranging from low- to high-level vision. We grouped the datasets (indicated in **bold**) into 3 broad categories (see following Sections) as illustrated by the images from 9 experiments in Figure 1. For examples of images from all 30 experiments see Appendix A. Each dataset comprised multiple sub-conditions designed to test DNN-human similarities, and in some cases, image datasets used to train decoders, as described in Section 3.3.

While most of the stimuli are created by us, in a few instances we incorporate stimuli from external sources (when needed, permission was obtained from the authors). In all cases, the stimuli have been integrated into a versatile framework which offers significant flexibility in adjusting parameters such as image size, background, stroke colour, and more, to allow their application to a variety of models and methodologies. Given the extensive range of datasets provided, we only offer a brief summary for each in the article, and provide more details in Appendix A, including details about the suggested way to test each dataset, and the expected result for model-human perceptual alignment. All resources are open-source and freely available under the MIT license at <https://github.com/MindSetVision/MindSetVision> and <https://github.com/miltonllera/mindset-eval> with additional Kaggle links to datasets we generated provided in the first repository’s README.

### 2.1 Low and Mid-Level Vision

A fundamental low-level vision phenomena is captured by **Weber’s Law** [26], which states that the minimum physical change of a stimulus on some dimension (e.g., its size) that is noticeable to an observer is a constant ratio of the original stimulus value on this dimension. For example, it is equally easy to distinguish between line lengths of 1 and 2 cms and between 2 and 4 cms. We created a dataset that can be used to assess this relation for both line length and stimulus intensity.

Human perception is also sensitive to various **Emergent Features** in which simple image features interact to generate “Gestalts” [27]. The dataset is comprised of a set of dots arranged in such a way as to induce the emergent feature of proximity, orientation, and linearity [28, 29]. Another Gestalt effect is manifest in the **Crowding/Uncrowding** phenomenon. In crowding, the ability to identify an object is compromised by the presence of nearby objects or visual patterns, but in uncrowding, object identification is improved when additional objects or visual patterns are added to the scene and grouped such that they are segregated from the target. We adapt the dataset from [30] so that many crowding conditions with several different shapes can be investigated.

Human perception is highly sensitive to non-accidental image features, that is features that are largely invariant to changes in viewpoint when projected on to the retina [31], as opposite to accidental features (e.g., degree of curvature) in which the projected image varies with viewpoint. Human vision is known to be more sensitive to changes in images that alter non-accidental compared to accidental properties [32, 33]. We use two datasets to examine model sensitivity to these features: one with **3D geons** [32] and another with **2D line segments** [based on 34]. Similarly, we present a dataset to compare **Relational Changes** with **Coordinate changes** between object parts. DNNs are commonly

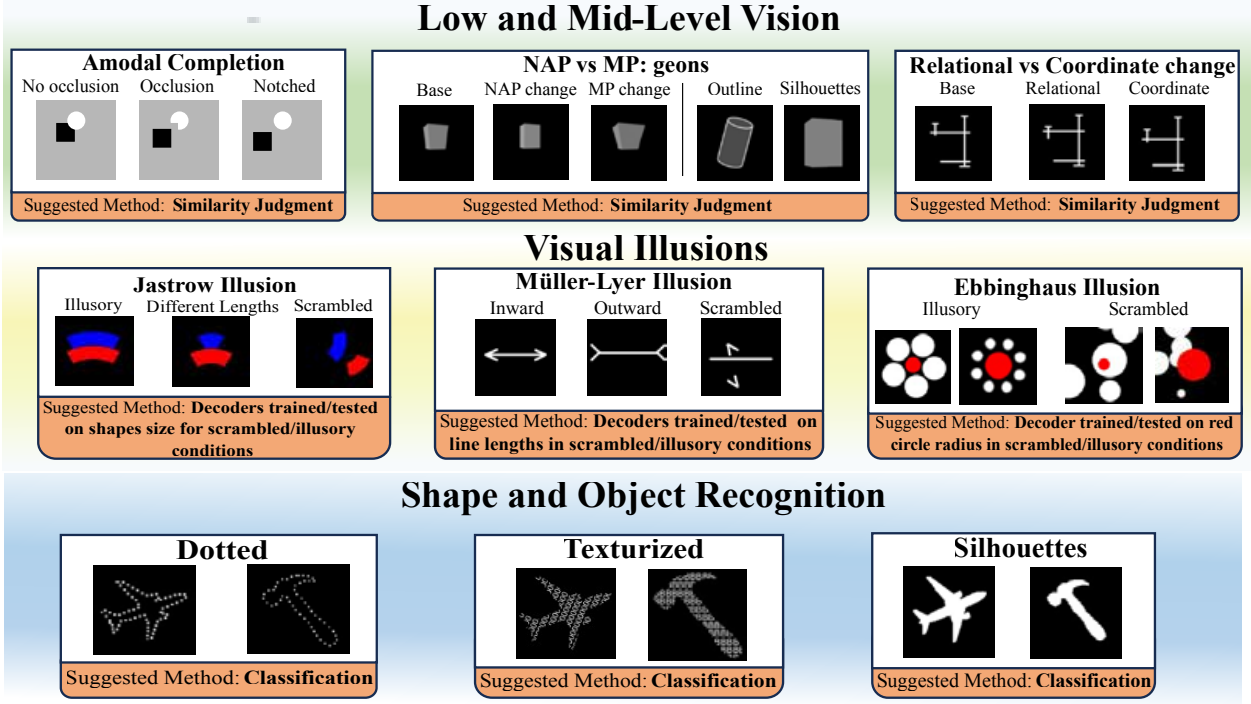


Figure 1: Illustration of experimental images included in the ‘MindSet: Vision’ datasets, arranged into three general categories of vision (see Appendix A for a full figure with all the datasets). Each panel includes images from a specific experiment, which is further divided into conditions.

insensitive to relational change, even after being explicitly trained on these relations [35], whereas human perception is highly sensitive to relational changes [36].

To identify partly occluded objects, the human visual system groups contours and surfaces through an amodal completion process [37]. The **Amodal Completion** dataset [based on 38] enables the investigation of these processes using images with shapes that are either occluded, unoccluded, or “notched”. These latter shapes are unoccluded but notched in such a way as to maintain a high degree of feature similarity with their occluded counterparts.

With the **Decomposition** dataset we provide a mean to test the extent to which DNNs group object parts in a human-like fashion. We designed familiar and unfamiliar objects composed of two conjoined parts that undergo what humans would perceive as a “natural” or “unnatural” break [inspired by 39]. In the same work, [39] showed that VGG-16 trained on ImageNet did not possess human-like sensitivity to images that could be interpreted as 3D-shapes by using a set of stimuli based on [40]. Accordingly, we reconstructed this **Depth Drawings** dataset.

## 2.2 Visual Illusions

Visual illusions are not mere curiosities, but often arise from adaptive perceptual processes [41]. Detailed computational models of multiple illusions have been advanced providing theoretical insights into the mechanisms that underlie them [e.g., 42]. We provide datasets exploring illusions related to size perception, orientation, and lightness contrast.

Several illusions relate to size perception. In the **Müller-Lyer illusion** [43], arrow-like segments at the ends of equal-length lines impact our perception of length. In the **Ponzo illusion** [44], two equal-length horizontal lines cross a pair of converging lines. In this configuration, the top line looks longer, an illusion often explained as related to the process of inferring depth. In the **Ebbinghaus illusion** [45], the size of a circle is perceived differently depending on the size of surrounding circles. Similarly, in the **Jastrow illusion** [43, 46], a specific arrangement of identical objects affects our perception of their relative size. For all these illusions, we provide both an illusory condition and a condition in which all elements of the original illusion are “scrambled up”, so that a decoder can be trained to predict a specific feature (e.g. the size of the centre circle in the Ebbinghaus illusion) and subsequently tested on illusory configurations.

In the **Tilt illusion** [47], the orientation of a central grating is perceived as being repulsed from or attracted to the orientation of a surrounding grating. In this case, we provide conditions with either central or background gratings (configurations which do not support the illusion in humans and could be used for training a decoder), and a condition

with both (eliciting the illusion in humans) for testing the model. Another orientation illusion is the **Thatcher Effect** [48]. This is a phenomenon where local changes in facial features (like inverted eyes or mouth) are less noticeable when the entire face is upside down, highlighting our sensitivity to orientation in face perception. An interesting unresolved issue is the extent to which this inversion effect is specific to faces [49, 50]. Together with a dataset of faces and their Thatcherized version, we also include a dataset of **Thatcherized Words**, that is a dataset of images containing words in which one or more letters are rotated by 180 degrees [50].

The **lightness contrast effect** [51] and the **Adelson Checker shadow** [52] illusions reveal how our visual system perceives color and lightness based on context. We provide a **Grayscale Shapes dataset** to train a decoder to output estimates of lightness at a given location of an image (indicated by a small white arrow). After training, the network is presented with test images that induce illusions and help assess whether DNNs show similar effects by pointing the arrow at the relevant parts of the images (see Appendix A.2.6 for a detailed description of this approach).

It is important to note that there is no accepted account for some of the illusions described above. However, even when we have no good understanding of the functional role or the mechanism that drives an illusion, a DNN model of human vision should show similar effect. Indeed, understanding the conditions under which DNNs show an illusion may advance our understanding of why the phenomenon is observed in humans. There are now several articles exploring such illusions in various types of DNNs trained in different ways, with some highlighting similarities [e.g., 53–55] others reporting mixed or discrepant results [e.g., 23, 56, 57]; for a review of the relevant findings, see [18].

### 2.3 Shape and Object Recognition

DNN object recognition is much more sensitive than human vision to distributional shifts from the training set. For instance, humans can easily identify line drawings the first time they are exposed to them [58], whereas DNNs perform poorly under these conditions [59] and need to be trained on line drawings in order to recognize them at human levels [60]. We have included the **line drawing** and **silhouettes** datasets [from 61, 62] and also manipulated them in various ways to construct additional datasets. The line drawings were converted into dotted contours (**Dotted line drawings**), line segments (**Segments line drawings**) [63], or “texturized” (**Texturized line drawings**). The texturized images are composed of oriented lines/characters applied to either/both the background or/and the inside area of the line drawing. In all these cases, the resulting images are easily identifiable by human observers due to various Gestalt rules that organize the image features into boundaries. We also apply the same texturization technique outlined above on unfamiliar “blob”-like shapes (**Texturized Unfamiliar dataset**). Human observers have no difficulty matching a novel “blob” object to its texturized counterpart. In addition, we provide a dataset of fragmented images based on [62] in which the global features of silhouettes or line drawing are modified by reflecting the top part of an object along its vertical axis, leaving the local features mostly unchanged (**Global Modifications** dataset). Human performance on these stimuli is greatly reduced but typically DNN performance is largely unchanged, suggesting that human vision is more sensitive to global object structure and DNN vision is more sensitive to local features.

The **Embedded Shapes Dataset** [inspired by 64] provides another condition that greatly impacts on human perception, by embedding geometric shapes within complex arrays of lines in ways that camouflage the original shape. We include both the original images from [64] and a procedurally generated dataset in which random polygons are embedded into a configuration that makes recognition challenging for humans.

The human visual system supports object recognition following a wide variety of transformations [65, 66]. Importantly, this extends to cases in which an object has only been viewed at one pose. Previous works suggest a complex link between DNN pretraining and their object recognition capabilities under object transformations [67, 68]. To test whether DNNs share these capacities, we provide a dataset in which translations, plane rotations, and scale changes (**2D Transformations**) are applied to line drawings. To test for **Viewpoint Invariance** (e.g. the ability to recognize an object from a new viewpoint after a rotation in depth) we adapt the ETH-80 dataset, [69] allowing for controlled variation in azimuth and inclination.

Finally, we provide a dataset to test whether DNNs possess the ability to solve a basic form of visual reasoning task, namely, the **Same/Different** task. Drawing from [70], our dataset comprises images composed of pairs of objects, which may be identical or different. These images are organized into ten conditions that vary in their visual form, such as ‘filled polygons’, ‘open squares’, and ‘colored shapes’. While humans effortlessly accomplish this task across all conditions without training, DNNs often struggle when the training and test images come from different conditions.

## 3 Testing methods

Each dataset is designed to align with at least one of three methods of testing, but other approaches can be used as well. We discuss further possibilities in Appendix D.3.

### 3.1 Out-of-Distribution Classification

In this approach, a DNN pretrained on one dataset is tested on a new dataset composed of out-of-distribution images taken from the trained classes (e.g., a DNN pre-trained on ImageNet is tested on line drawings taken from the same categories). This approach is well suited for most of the Shape and Object Recognition datasets that use images from ImageNet categories modified in such a way that human observers have no trouble recognizing them, even without training. We provide scripts to test a wide variety of vision models.

### 3.2 Similarity Judgment Analysis

This method involves assessing the pairwise similarity of activation patterns in DNNs (using a Cosine Similarity or an Euclidean Distance metric) evoked by pairs of images. This method has been used to assess how well DNNs capture human similarity judgments [9] and response times to identify target stimuli from foils [29]. It is often useful to carry out these analyses across multiple layers of DNNs given that some psychological phenomena are known to manifest at earlier or later stages of visual processing. A DNN mimicking human perception should show relevant similarity effects at the relevant layers. This method is appropriate when comparing the similarity of the complete images presented to the network. One key advantage of this approach is that it can be applied to novel images that cannot be classified by a DNN.

### 3.3 Decoder Method

In this method a small, often single-layer, “decoder” network is attached to a layer of a frozen DNN and trained on a task designed to reveal how the DNN encodes a specific type of information. For instance, a frozen DNN might be presented with a set of images that contain a target object varying in size, colour, and orientation, and a decoder is trained to output the value of one or more of these properties at a given layer. We provide methods for both classification and regression training. Currently, these linear probes attach to all linear and convolution layers in a network. While generic, it serves as an easy to understand blueprint for more targeted approaches. This method is appropriate when assessing whether networks are processing specific components of an image (e.g., central circle in the Ebbinghaus Illusion) in a human-like way.

## 4 Models

We tested 15 DNNs on 9 experiments from the toolkit. These models were picked so as to cover a variety of architectures. Thus we picked two (2) ResNets, two (2) ResNexts, three (3) ConvNexts, three (3) ViTs, three (3) DEITs and (2) FocalNets. Within each group we picked variants with varying parameter counts and training settings (specifically training datasets, such as ones using CLIP and others using LAION). Except for the FocalNets, which have not been tested, all models achieve high scores on the BrainScore. Indeed, the two large convent models are the two highest scoring models at the moment on both behavioural and neural ranks. More details can be found Appendix C.

## 5 Results

We present results from 9 datasets here. In the main text we only present results from the layer in each network with the largest effect (difference between conditions) which is an approach similar to measuring network alignment with neural activity (like BrainScore) where the layer explaining the most variance is taken as the network score. For more detailed analyses and figures, see Appendix E. For the out-of-distribution classification tasks, we chose top-5 accuracy as the measure of performance.

The networks we tested showed a human-like pattern of results in some of the experimental conditions, and failed to in others. Network responses showed evidence for amodal completion and a sensitivity to non-accidental properties. Most networks also estimated the size of a bottom arc in the Jastrow illusion as larger than the top one (as humans do) although the magnitude of some of these estimates is quite unhuman-like (i.e. 10x the actual size). But it is important to note that pattern of results across layers of the networks was often quite variable, and some these correspondences break down when more detailed analyses carried out (see Appendix E). The other results reported above reveal striking discrepancies between DNNs and humans. Networks consistently failed to show evidence of the Müller-Lyer illusion, and mixed evidence for the Ebbinghaus illusion. Further, DNNs did not show human sensitivity to the relations between object parts, and the classification performance on the out-of-distribution images that requires the extraction of shape did not approach human performance.

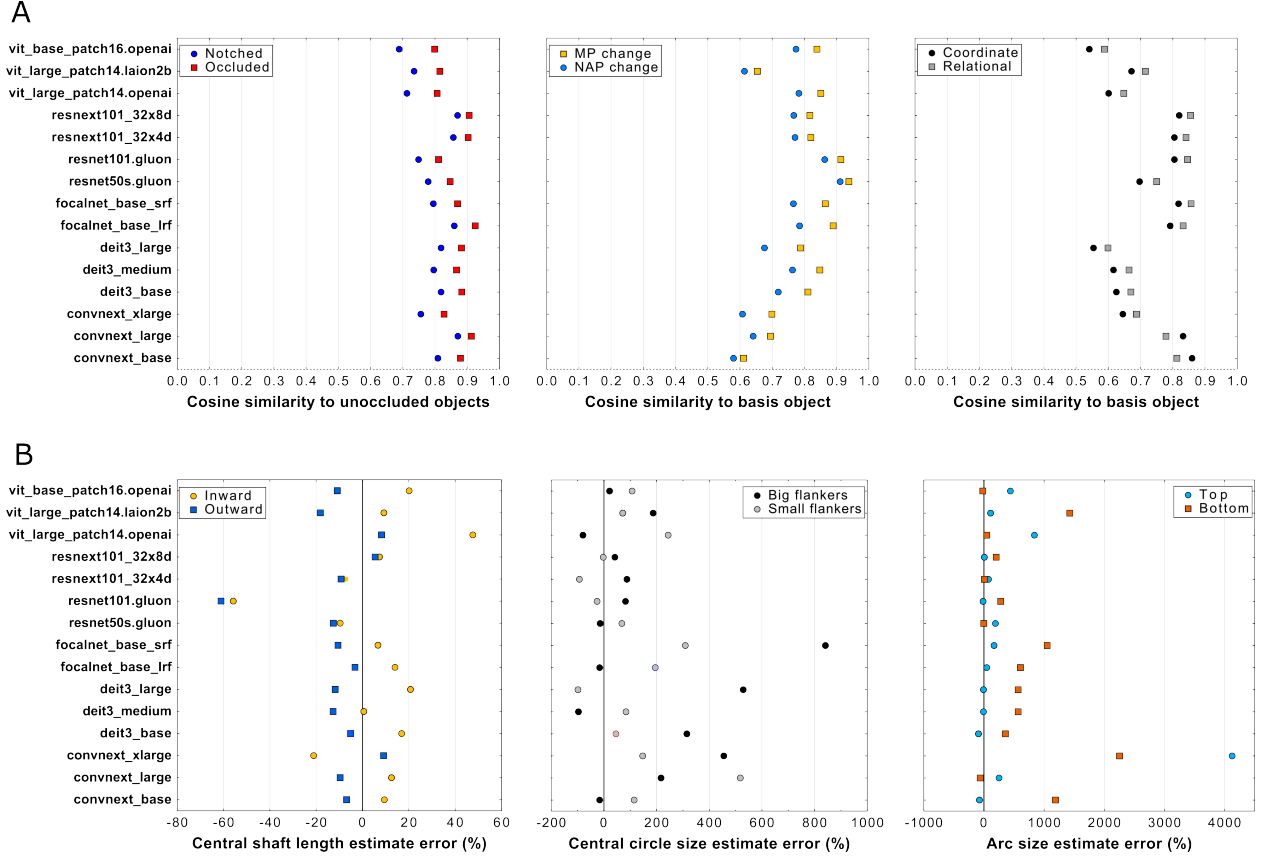


Figure 2: Results from similarity (A) and decoding (B) methods. For human-like results in (A), the similarity for Occluded compared to Notched stimuli should be higher when compared to Unoccluded objects, due to amodal completion, as found (left). The similarity for metric properties (MP) compared to non-accidental properties (NAP) stimuli should be higher compared to base objects, as found (center). The similarity for coordinate compared to relational stimuli should be higher when compared to basis objects, as not found (right). For human-like results in (B), the central shaft should be estimated as longer in configurations with outward compared to inward facing fins due to the Müller-Lyer illusion, which was not found in most cases (left). Central circles should be estimated as larger when surrounded by smaller compared to larger flankers due to the Ebbinghaus illusion, with mixed results obtained (center). Bottom arcs should be estimated as longer than top arcs when they are the same length in a vertically aligned configuration due to the Jastrow illusion, which was found in majority cases (right). Reference line at 0 would represent perfectly correct estimates.

## 6 Code and Resources

We provide both ready-to-use datasets and scripts to generate them with varying parameters. Most of the ready-to-use datasets’ size span to around 5,000 images per condition, and larger dataset can easily be generated using the provided scripts. To separate code and configuration, each dataset generation script relies on a configuration file, consisting of a plain-text file in TOML format specifying all the available parameters for that dataset. Some parameters are used across most datasets, such as image size, background colour, and number of samples. Other parameters are dataset-specific, for example the size and distance of dots in the Dotted line drawing dataset. For convenience, the same configuration file can specify the configuration for multiple (or all) datasets, so that they can be generated in batches. The “default” configuration file we used to generate the ready-to-use versions is included, which can be used as a template. The output of each script is the dataset itself (with several sub-conditions depending on the dataset) together with a CSV annotation file, containing the path and parameters of each generated image.

We also provide the code and utilities to evaluate DNNs using the three methods noted above. Each method is highly configurable through TOML files, with options including the type of data-augmentation to apply, the network architecture, the metric to use for the similarity judgments and more. Users have the flexibility to choose specific factors from this file for analysis, extending beyond the factors that we deemed the most relevant for each task. For example,

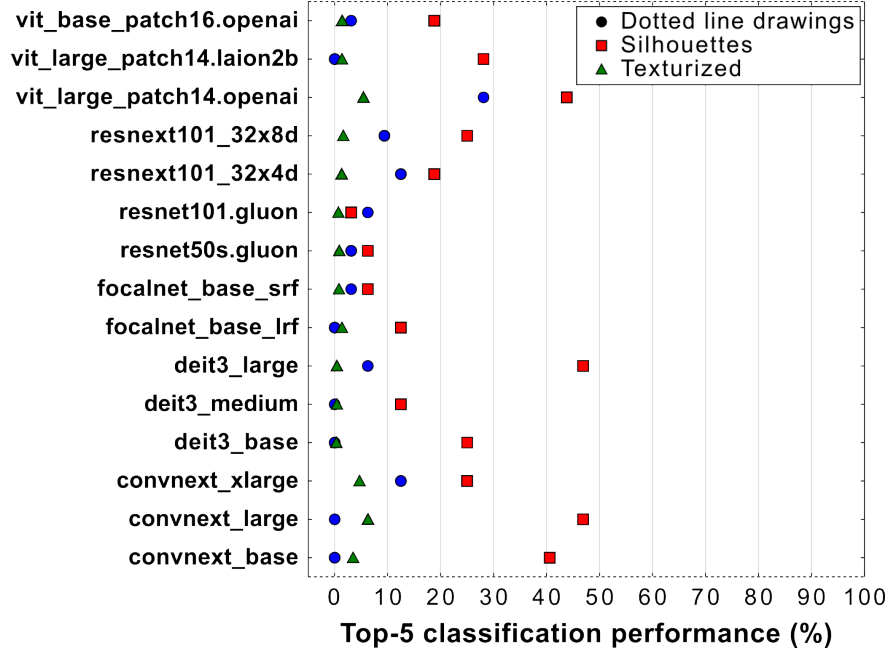


Figure 3: Out of distribution classification results. Human performance in all of three conditions is over 90%.

in the script testing the Ebbinghaus Illusion used for Section 3.3, a decoder is trained to predict the normalized size of the centre circle. However, a different research goal might involve predicting the size of the flankers. This can be achieved by simply specifying the corresponding column ('NormSizeFlankers') in the annotation file, without needing to re-generate the dataset or change the code.

Each method produces pandas DataFrames [71] as its output, which can be independently analyzed. Supplementary files containing simple tests and comparisons that serve as a springboard for further and more detailed analysis are automatically generated. We provide documentation for every configurable option across all datasets and methods and offer guidance on the general usage of various scripts and utilities through several examples and multiple README files on the GitHub page.

## 7 Limitations

There are three limitations of our work we would like to mention. First, we have only tested DNNs on 9 of the 30 experiments in the toolkit. We think this is appropriate given the goal of our simulation studies was to highlight the value of testing DNNs on psychological experiments. Although we have shown that DNNs that perform well on the Brain-Score benchmark struggle to account for a number of experiments in our toolkit, we have no doubt that DNNs can be built to succeed on many of these tasks. Our simulations are intended to motivate further research in this direction and our toolkit is designed to make this easier. Second, we have not provided behavioural datasets for the 30 experiments that would allow researchers to assess the overall variance accounted for. This would be a useful addition, but it is important to note that our toolkit only includes stimuli from experiments that manipulate independent variables. The qualitative effects of all the manipulations in the 30 experiments are well-known, theoretically significant, and robust. Accordingly, DNNs can already be meaningfully tested on all the experiments in our toolkit. It is also worth noting that there is a danger of providing a behavioural benchmark for each experiment, as it will encourage researchers to compete on this dataset rather than design a range of experiments on a given visual phenomenon to provide severe tests DNN-brain alignment. Indeed, relying on a single behavioural dataset per experiment is problematic given the replication crisis in psychology (and other fields). Third, we have only provided a superficial analyses of the models on nine experiments. More detailed analyses and additional experiments may reveal additional strengths or weakness of the models, and our toolkit will facilitate this line of research.

## 8 Conclusion

There is much interest in DNNs as models of human vision, but relatively little research is concerned with how DNNs capture key psychological findings. When DNNs are tested against key psychological findings, they often fail [19]. And when they do succeed, it is often because the DNNs have not been severely tested [20]. In our view, to better characterize DNN-human alignment, and to build better DNN models of human vision, it is necessary to systematically test models against key experiments reported in psychology. The MindSet: Vision toolkit is designed to facilitate this.

We also demonstrated the value of our toolkit by testing 15 DNNs on 9 experiments, ranging from relatively low-level vision (e.g., amodal completion) to object recognition (classifying dotted line-drawings). The key take-home message from these simulation studies is that all models struggled on many of the experiments. Importantly, we do not see the current failures of DNNs on some of the psychological studies included in our toolkit as undermining the importance of DNNs for understanding human vision (and other aspects of human intelligence). Rather, the toolkit can be used to better understand the strengths and weaknesses of current DNNs as models of biological vision, with the ultimate goal of building more aligned DNNs to better understand human vision [35]. This will no doubt require many simulation studies and multiple articles devoted to each phenomenon to better assess DNN-human alignment (similar to the wide range of psychological studies devoted to each phenomenon). This is a quite different approach compared to common practice of assessing how much overall variance DNNs account for on a small set of observational benchmark datasets.

### Acknowledgments

This project has received funding from the European Research Council (ERC) under the European Union’s Horizon 2020 research and innovation programme (grant agreement No 741134). Guillermo Puebla has also received funding for this project from the National Center for Artificial Intelligence CENIA FB210017, Basal ANID.

## References

- [1] Jonas Kubilius, Martin Schrimpf, Kohitij Kar, Rishi Rajalingham, Ha Hong, Najib J Majaj, Elias B Issa, Pouya Bashivan, Jonathan Prescott-Roy, Kailyn Schmidt, Aran Nayebi, Daniel Bear, Daniel L K Yamins, and James J Dicarlo. Brain-Like Object Recognition with High-Performing Shallow Recurrent ANNs. *33rd Conference on Neural Information Processing Systems (NeurIPS 2019)*, 2019.
- [2] Johannes Mehrer, Courtney J. Spoerer, Emer C. Jones, Nikolaus Kriegeskorte, and Tim C. Kietzmann. An ecologically motivated image dataset for deep learning yields better models of human vision. *Proceedings of the National Academy of Sciences*, 118(8), February 2021. ISSN 0027-8424. doi: 10.1073/PNAS.2011417118.
- [3] Chengxu Zhuang, Siming Yan, Aran Nayebi, Martin Schrimpf, Michael C. Frank, James J. DiCarlo, and Daniel L. K. Yamins. Unsupervised Neural Network Models of the Ventral Visual Stream. *bioRxiv*, page 2020.06.16.155556, 2020. doi: 10.1101/2020.06.16.155556.
- [4] James J. Dicarlo, Daniel L.K. Yamins, Michael E. Ferguson, Evelina Fedorenko, Matthias Bethge, Tyler Bonnen, and Martin Schrimpf. Let’s move forward: Image-computable models and a common model evaluation scheme are prerequisites for a scientific understanding of human vision. *The Behavioral and brain sciences*, 46, December 2023. ISSN 1469-1825. doi: 10.1017/S0140525X23001607.
- [5] Tal Golan, Johnmark Taylor, Heiko Schütt, Benjamin Peters, Rowan P. Sommers, Katja Seeliger, Adrien Doerig, Paul Linton, Talia Konkle, Marcel Van Gerven, Konrad Kording, Blake Richards, Tim C. Kietzmann, Grace W. Lindsay, and Nikolaus Kriegeskorte. Deep neural networks are not a single hypothesis but a language for expressing computational hypotheses. *The Behavioral and brain sciences*, 46, December 2023. ISSN 1469-1825. doi: 10.1017/S0140525X23001553.
- [6] Rishi Rajalingham, Elias B. Issa, Pouya Bashivan, Kohitij Kar, Kailyn Schmidt, and James J. DiCarlo. Large-Scale, High-Resolution Comparison of the Core Visual Object Recognition Behavior of Humans, Monkeys, and State-of-the-Art Deep Artificial Neural Networks. *Journal of Neuroscience*, 38(33):7255–7269, August 2018. ISSN 0270-6474. doi: 10.1523/JNEUROSCI.0388-18.2018.
- [7] Shikhar Tuli, Ishita Dasgupta, Erin Grant, and Thomas L. Griffiths. Are Convolutional Neural Networks or Transformers more like human vision? *Proceedings of the 43rd Annual Meeting of the Cognitive Science Society: Comparative Cognition: Animal Minds, CogSci 2021*, pages 1844–1850, May 2021. doi: 10.48550/arxiv.2105.07197.
- [8] M. N. Hebart, O. Contier, L. Teichmann, A. H. Rockter, C. Y. Zheng, A. Kidder, A. Corriveau, M. Vaziri-Pashkam, and C. I. Baker. THINGS-data, a multimodal collection of large-scale datasets for investigating object representations in human brain and behavior. *eLife*, 12, February 2023. ISSN 2050084X. doi: 10.7554/ELIFE.82580.
- [9] Joshua C. Peterson, Joshua T. Abbott, and Thomas L. Griffiths. Evaluating (and improving) the correspondence between deep neural networks and human representations. *Cognitive Science*, 42(8):2648–2669, June 2017. ISSN 15516709. doi: 10.1111/cogs.12670.
- [10] Ruairidh M. Battleday, Joshua C. Peterson, and Thomas L. Griffiths. Capturing human categorization of natural images by combining deep networks and cognitive models. *Nature Communications 2020 11:1*, 11(1):1–14, October 2020. ISSN 2041-1723. doi: 10.1038/s41467-020-18946-z.
- [11] Martin Schrimpf, Jonas Kubilius, Ha Hong, Najib J. Majaj, Rishi Rajalingham, Elias B. Issa, Kohitij Kar, Pouya Bashivan, Jonathan Prescott-Roy, Kailyn Schmidt, Daniel L. K. Yamins, and James J. DiCarlo. Brain-Score: Which Artificial Neural Network for Object Recognition is most Brain-Like? *bioRxiv*, page 407007, September 2018. doi: 10.1101/407007.
- [12] Martin Schrimpf, Jonas Kubilius, Michael J. Lee, N. Apurva Ratan Murty, Robert Ajemian, and James J. DiCarlo. Integrative Benchmarking to Advance Neurally Mechanistic Models of Human Intelligence. *Neuron*, 108(3): 413–423, November 2020. ISSN 0896-6273. doi: 10.1016/J.NEURON.2020.07.040.
- [13] Emily J. Allen, Ghislain St-Yves, Yihan Wu, Jesse L. Breedlove, Jacob S. Prince, Logan T. Dowdle, Matthias Nau, Brad Caron, Franco Pestilli, Ian Charest, J. Benjamin Hutchinson, Thomas Naselaris, and Kendrick Kay. A massive 7T fMRI dataset to bridge cognitive neuroscience and artificial intelligence. *Nature neuroscience*, 25(1): 116–126, January 2022. ISSN 1546-1726. doi: 10.1038/S41593-021-00962-X.

- [14] Nikolaus Kriegeskorte, Marieke Mur, Douglas A. Ruff, Roozbeh Kiani, Jerzy Bodurka, Hossein Esteky, Keiji Tanaka, and Peter A. Bandettini. Matching categorical object representations in inferior temporal cortex of man and monkey. *Neuron*, 60(6):1126–1141, December 2008. ISSN 1097-4199. doi: 10.1016/J.NEURON.2008.10.043.
- [15] Charles F. Cadieu, Ha Hong, Daniel L.K. Yamins, Nicolas Pinto, Diego Ardila, Ethan A. Solomon, Najib J. Majaj, and James J. DiCarlo. Deep Neural Networks Rival the Representation of Primate IT Cortex for Core Visual Object Recognition. *PLOS Computational Biology*, 10(12):e1003963, December 2014. ISSN 1553-7358. doi: 10.1371/JOURNAL.PCBI.1003963.
- [16] Marin Dujmović, Jeffrey Bowers, Federico Adolphi, and Gaurav Malhotra. Inferring DNN-Brain alignment using representational similarity analyses can be problematic. In *ICLR 2024 Workshop on Representational Alignment*, 2024. URL <https://openreview.net/forum?id=dSEwiAENTS>.
- [17] Gaurav Malhotra and Jeff Bowers. Predicting brain activation does not license conclusions regarding dnn-brain alignment: The case of brain-score. Poster presented at Cognitive Computational Neuroscience (CCN), Poster Session B, Boston, USA, 2024. URL <https://2024.ccneuro.org/poster/?id=156>. Poster ID: B81.
- [18] Nancy Kanwisher, Meenakshi Khosla, and Katharina Dobs. Using artificial neural networks to ask ‘why’ questions of minds and brains. *Trends in Neurosciences*, 46(3):240–254, March 2023. ISSN 0166-2236, 1878-108X. doi: 10.1016/j.tins.2022.12.008.
- [19] Jeffrey S. Bowers, Gaurav Malhotra, Marin Dujmović, Milton Llera Montero, Christian Tsvetkov, Valerio Biscione, Guillermo Puebla, Federico Adolphi, John E. Hummel, Rachel F. Heaton, Benjamin D. Evans, Jeffrey Mitchell, and Ryan Blything. Deep Problems with Neural Network Models of Human Vision. *Behavioral and Brain Sciences*, pages 1–74, December 2023. ISSN 0140-525X. doi: 10.1017/S0140525X22002813.
- [20] Jeffrey S. Bowers, Gaurav Malhotra, Federico Adolphi, Marin Dujmović, Milton L. Montero, Valerio Biscione, Guillermo Puebla, John H. Hummel, and Rachel F. Heaton. On the importance of severely testing deep learning models of cognition. *Cognitive Systems Research*, 82:101158, December 2023. ISSN 1389-0417. doi: 10.1016/J.COGSYS.2023.101158.
- [21] Monya Baker. Over half of psychology studies fail reproducibility test. *Nature*, August 2015. ISSN 1476-4687. doi: 10.1038/nature.2015.18248.
- [22] Aniket Roy, Anirban Roy, Soma Mitra, and Kuntal Ghosh. Bri3l: A brightness illusion image dataset for identification and localization of regions of illusory perception. In *2024 IEEE International Conference on Image Processing (ICIP)*, pages 62–68, 2024. doi: 10.1109/ICIP51287.2024.10647946.
- [23] Yichi Zhang, Jiayi Pan, Yuchen Zhou, Rui Pan, and Joyce Chai. Grounding visual illusions in language: Do vision-language models perceive illusions like humans? In Houda Bouamor, Juan Pino, and Kalika Bali, editors, *Proceedings of the 2023 Conference on Empirical Methods in Natural Language Processing*, pages 5718–5728, Singapore, December 2023. Association for Computational Linguistics. doi: 10.18653/v1/2023.emnlp-main.348. URL <https://aclanthology.org/2023.emnlp-main.348>.
- [24] Ben Lonnqvist, Zhengqing Wu, and Michael Herzog. Latent noise segmentation: How neural noise leads to the emergence of segmentation and grouping. In Ruslan Salakhutdinov, Zico Kolter, Katherine Heller, Adrian Weller, Nuria Oliver, Jonathan Scarlett, and Felix Berkenkamp, editors, *Proceedings of the 41st International Conference on Machine Learning*, volume 235 of *Proceedings of Machine Learning Research*, pages 32726–32758. PMLR, 21–27 Jul 2024. URL <https://proceedings.mlr.press/v235/lonnqvist24a.html>.
- [25] Robert Geirhos, Kantharaju Narayanappa, Benjamin Mitzkus, Tizian Thieringer, Matthias Bethge, Felix A. Wichmann, and Wieland Brendel. Partial success in closing the gap between human and machine vision. In A. Beygelzimer, Y. Dauphin, P. Liang, and J. Wortman Vaughan, editors, *Advances in Neural Information Processing Systems*, 2021. URL <https://openreview.net/forum?id=QkljT4mrfs>.
- [26] E. H. Weber. Der Tastsinn und das Gemeingefühl. *Handwörterbuch der Physiologie*, 3:481–588, 1983.
- [27] James R. Pomerantz and Mary C. Portillo. Grouping and Emergent Features in Vision: Toward a Theory of Basic Gestalts. *Journal of Experimental Psychology: Human Perception and Performance*, 37(5):1331–1349, October 2011. ISSN 00961523. doi: 10.1037/A0024330.

- [28] James R. Pomerantz and Mary C. Portillo. Grouping and emergent features in vision: Toward a theory of basic Gestalts. *Journal of experimental psychology. Human perception and performance*, 37(5):1331–1349, October 2011. ISSN 1939-1277. doi: 10.1037/A0024330.
- [29] Valerio Biscione and Jeffrey S. Bowers. Mixed Evidence for Gestalt Grouping in Deep Neural Networks. *Computational Brain and Behavior*, 6(3):438–456, September 2023. ISSN 2522087X. doi: 10.1007/S42113-023-00169-2/.
- [30] Adrien Doerig, Alban Bornet, Ruth Rosenholtz, Gregory Francis, Aaron M. Clarke, and Michael H. Herzog. Beyond Bouma’s window: How to explain global aspects of crowding? *PLOS Computational Biology*, 15(5): e1006580, May 2019. ISSN 1553-7358. doi: 10.1371/JOURNAL.PCBI.1006580.
- [31] Irving Biederman. Recognition-by-Components: A Theory of Human Image Understanding. *Psychological Review*, 94(2):115–147, 1987. ISSN 0033295X. doi: 10.1037/0033-295X.94.2.115.
- [32] Ori Amir, Irving Biederman, and Kenneth J. Hayworth. Sensitivity to nonaccidental properties across various shape dimensions. *Vision Research*, 62:35–43, June 2012. ISSN 0042-6989. doi: 10.1016/j.visres.2012.03.020.
- [33] Ori Amir, Irving Biederman, Sarah B. Herald, Manan P. Shah, and Toben H. Mintz. Greater sensitivity to nonaccidental than metric shape properties in preschool children. *Vision Research*, 97:83–88, 2014. ISSN 18785646. doi: 10.1016/J.VISRES.2014.02.006.
- [34] Jonas Kubilius, Charlotte Sleurs, and Johan Wagemans. Sensitivity to nonaccidental configurations of two-line stimuli. *i-Perception*, 8(2):1–12, April 2017. ISSN 20416695. doi: 10.1177/2041669517699628/ASSET/IMAGES/LARGE/10.1177\_2041669517699628-FIG2.JPEG.
- [35] Gaurav Malhotra, Marin Dujmović, John Hummel, and Jeffrey S. Bowers. Human shape representations are not an emergent property of learning to classify objects. *Journal of Experimental Psychology: General*, 152(12): 3380–3402, 2023. doi: 10.1037/xge0001440. URL <https://doi.org/10.1037/xge0001440>.
- [36] John E. Hummel and Brian J. Stankiewicz. Categorical relations in shape perception. *Spatial Vision*, 10(3): 201–236, 1996. ISSN 01691015. doi: 10.1163/156856896X00141.
- [37] Ken Nakayama and Shinsuke Shimojo. Experiencing and Perceiving Visual Surfaces. *Science*, 257(5075): 1357–1363, September 1992. ISSN 0036-8075. doi: 10.1126/SCIENCE.1529336.
- [38] Ronald A. Rensink and James T. Enns. Early completion of occluded objects. *Vision Research*, 38(15-16): 2489–2505, August 1998. ISSN 0042-6989. doi: 10.1016/S0042-6989(98)00051-0.
- [39] Georgin Jacob, R. T. Pramod, Harish Katti, and S. P. Arun. Qualitative similarities and differences in visual object representations between brains and deep networks. *Nature Communications* 2021 12:1, 12(1):1–14, March 2021. ISSN 2041-1723. doi: 10.1038/s41467-021-22078-3.
- [40] James T. Enns and Ronald A. Rensink. Preattentive recovery of three-dimensional orientation from line drawings. *Psychological review*, 98(3):335–351, 1991. ISSN 0033-295X. doi: 10.1037/0033-295X.98.3.335.
- [41] Richard L. Gregory. Knowledge in perception and illusion. *Philosophical Transactions of the Royal Society B: Biological Sciences*, 352(1358):1121, August 1997. ISSN 09628436. doi: 10.1098/RSTB.1997.0095.
- [42] Stephen Grossberg. The visual world as illusion: The ones we know and the ones we don’t. In *The Oxford Compendium of Visual Illusions*, pages 90–118. Oxford University Press, New York, NY, US, 2017. ISBN 978-0-19-979460-7. doi: 10.1093/acprof:oso/9780199794607.003.0007.
- [43] R. H. Day and H. Knuth. The Contributions of F C Müller-Lyer. <http://dx.doi.org/10.1068/p100126>, 10(2): 126–146, April 1981. ISSN 03010066. doi: 10.1068/P100126.
- [44] Mario Ponzo. *Intorno ad alcune illusioni nel campo delle sensazioni tattili, sull’illusione di Aristotele e fenomeni analoghi*. Wilhelm Engelmann, 1910.
- [45] Salvatore Aglioti, Joseph F.X. DeSouza, and Melvyn A. Goodale. Size-contrast illusions deceive the eye but not the hand. *Current Biology*, 5(6):679–685, June 1995. ISSN 0960-9822. doi: 10.1016/S0960-9822(95)00133-3.
- [46] Joseph Jastrow. Studies from the Laboratory of Experimental Psychology of the University of Wisconsin. II. *The American Journal of Psychology*, 4(3):381–428, 1892. ISSN 0002-9556. doi: 10.2307/1411617.

- [47] J. J. Gibson and M. Radner. Adaptation, after-effect and contrast in the perception of tilted lines. *Journal of Experimental Psychology*, 20(5):453–467, May 1937. ISSN 00221015. doi: 10.1037/H0059826.
- [48] P. Thompson. Margaret Thatcher: A new illusion. *Perception*, 9(4):483–484, 1980. ISSN 03010066. doi: 10.1068/P090483.
- [49] Luc Boutsen, Glyn W. Humphreys, Peter Praamstra, and Tracy Warbrick. Comparing neural correlates of configural processing in faces and objects: An ERP study of the Thatcher illusion. *NeuroImage*, 32(1):352–367, August 2006. ISSN 10538119. doi: 10.1016/j.neuroimage.2006.03.023.
- [50] Yetta K Wong, Elyssa Twedt, David Sheinberg, and Isabel Gauthier. Does Thompson’s Thatcher Effect Reflect a Face-Specific Mechanism? *Perception*, 39(8):1125–1141, August 2010. ISSN 0301-0066. doi: 10.1068/p6659.
- [51] Hermann Von Helmholtz. *Handbuch der physiologischen Optik*, volume 9. Voss, 1867.
- [52] E. H. Adelson. Checkershadow Illusion. *Perceptual Science Group*, 2005.
- [53] Ari Benjamin, Cheng Qiu, Ling-Qi Zhang, Konrad Kording, and Alan Stocker. Shared visual illusions between humans and artificial neural networks. *2019 Conference on Cognitive Computational Neuroscience*, August 2019. doi: 10.32470/CCN.2019.1299-0.
- [54] Katherine R. Storrs, Barton L. Anderson, and Roland W. Fleming. Unsupervised learning predicts human perception and misperception of gloss. *Nature Human Behaviour* 2021 5:10, 5(10):1402–1417, May 2021. ISSN 2397-3374. doi: 10.1038/s41562-021-01097-6.
- [55] Eiji Watanabe, Akiyoshi Kitaoka, Kiwako Sakamoto, Masaki Yasugi, and Kenta Tanaka. Illusory Motion Reproduced by Deep Neural Networks Trained for Prediction. *Frontiers in Psychology*, 9, March 2018. ISSN 1664-1078. doi: 10.3389/fpsyg.2018.00345.
- [56] Alexander Gomez-Villa, Adrian Martin, Javier Vazquez-Corral, and Marcelo Bertalmio. Convolutional Neural Networks Can Be Deceived by Visual Illusions . In *2019 IEEE/CVF Conference on Computer Vision and Pattern Recognition (CVPR)*, pages 12301–12309, Los Alamitos, CA, USA, June 2019. IEEE Computer Society. doi: 10.1109/CVPR.2019.01259. URL <https://doi.ieeecomputersociety.org/10.1109/CVPR.2019.01259>.
- [57] Emily J Ward. Exploring perceptual illusions in deep neural networks. *Journal of Vision*, 19(10):34b–34b, September 2019. ISSN 1534-7362. doi: 10.1167/19.10.34B.
- [58] J. Hochberg and V. Brooks. Pictorial recognition as an unlearned ability: A study of one child’s performance. *The American journal of psychology*, 75:624–628, 1962. ISSN 00029556. doi: 10.2307/1420286.
- [59] Benjamin D. Evans, Gaurav Malhotra, and Jeffrey S. Bowers. Biological convolutions improve DNN robustness to noise and generalisation. *Neural Networks*, 148:96–110, April 2022. ISSN 0893-6080. doi: 10.1016/J.NEUNET.2021.12.005.
- [60] Johannes J.D. Singer, Katja Seeliger, Tim C. Kietzmann, and Martin N. Hebart. From photos to sketches - how humans and deep neural networks process objects across different levels of visual abstraction. *Journal of Vision*, 22(2):4–4, February 2022. ISSN 1534-7362. doi: 10.1167/JOV.22.2.4.
- [61] Nicholas Baker, Hongjing Lu, Gennady Erlikhman, and Philip J. Kellman. Deep convolutional networks do not classify based on global object shape. *PLoS Computational Biology*, 14(12):1–43, 2018. ISSN 15537358. doi: 10.1371/journal.pcbi.1006613.
- [62] Nicholas Baker and James H. Elder. Deep learning models fail to capture the configural nature of human shape perception. *iScience*, 25(9), September 2022. ISSN 2589-0042. doi: 10.1016/J.ISCI.2022.104913.
- [63] Irving Biederman and Eric E. Cooper. Priming contour-deleted images: Evidence for intermediate representations in visual object recognition. *Cognitive Psychology*, 23(3):393–419, July 1991. ISSN 0010-0285. doi: 10.1016/0010-0285(91)90014-F.
- [64] Lee de-Wit, Hanne Huygelier, Ruth Van der Hallen, Rebecca Chamberlain, and Johan Wagemans. Developing the Leuven Embedded Figures Test (L-EFT): Testing the stimulus features that influence embedding. *PeerJ*, 5, 2017. doi: 10.7717/peerj.2862.
- [65] Keiji Tanaka. Inferotemporal Cortex and Object Vision. *Annual Review of Neuroscience*, 19(1):109–139, March 1996. ISSN 0147-006X. doi: 10.1146/annurev.ne.19.030196.000545.

- [66] Ryan Blything, Valerio Biscione, Ivan I Vankov, Casimir J H Ludwig, and Jeffrey S Bowers. The human visual system and CNNs can both support robust online translation tolerance following extreme displacements. *Journal of Vision*, 21(2):1–16, 2021. doi: 10.1167/jov.21.2.9.
- [67] Valerio Biscione and Jeffrey S. Bowers. Convolutional Neural Networks Are Not Invariant to Translation, but They Can Learn to Be. *Journal of Machine Learning Research*, 22(229):1–28, 2021. ISSN 1533-7928.
- [68] Valerio Biscione and Jeffrey S. Bowers. Learning online visual invariances for novel objects via supervised and self-supervised training. *Neural Networks*, March 2022. ISSN 0893-6080. doi: 10.1016/J.NEUNET.2022.02.017.
- [69] Kai-Xuan Chen, Jie-Yi Ren, Xiao-Jun Wu, and Josef Kittler. Covariance descriptors on a Gaussian manifold and their application to image set classification. *Pattern Recognition*, 107:107463, November 2020. ISSN 0031-3203. doi: 10.1016/j.patcog.2020.107463.
- [70] Guillermo Puebla and Jeffrey S. Bowers. Can deep convolutional neural networks support relational reasoning in the same-different task? *Journal of Vision*, 22(10):11, September 2022. ISSN 1534-7362. doi: 10.1167/jov.22.10.11.
- [71] Wes McKinney. Data Structures for Statistical Computing in Python. In *Python in Science Conference*, pages 56–61, Austin, Texas, 2010. doi: 10.25080/Majora-92bf1922-00a.
- [72] Robert F. Hess and Anthony Hayes. Neural recruitment explains “weber’s law” of spatial position. *Vision Research*, 33(12):1673–1684, August 1993. ISSN 0042-6989. doi: 10.1016/0042-6989(93)90033-S.
- [73] H. B. Barlow. Optic nerve impulses and Weber’s law. *Cold Spring Harbor symposia on quantitative biology*, 30: 539–546, 1965. ISSN 0091-7451. doi: 10.1101/SQB.1965.030.01.052.
- [74] Daniel K. Freeman, Gilberto Graña, and Christopher L. Passaglia. Retinal Ganglion Cell Adaptation to Small Luminance Fluctuations. *Journal of Neurophysiology*, 104(2):704, August 2010. ISSN 00223077. doi: 10.1152/JN.00767.2009.
- [75] Michel Treisman. Noise and Weber’s law: The discrimination of brightness and other dimensions. *Psychological Review*, 71(4):314–330, July 1964. ISSN 0033295X. doi: 10.1037/H0042445.
- [76] Toni P. Saarela, Bilge Sayim, Gerald Westheimer, and Michael H. Herzog. Global stimulus configuration modulates crowding. *Journal of Vision*, 9(2):5–5, February 2009. ISSN 1534-7362. doi: 10.1167/9.2.5.
- [77] A. Doerig, A. Bornet, O. H. Choung, and M. H. Herzog. Crowding reveals fundamental differences in local vs. global processing in humans and machines. *Vision Research*, 167:39–45, February 2020. ISSN 0042-6989. doi: 10.1016/j.visres.2019.12.006.
- [78] Gregory Francis, Mauro Manassi, and Michael H. Herzog. Neural dynamics of grouping and segmentation explain properties of visual crowding. *Psychological Review*, 124(4):483–504, July 2017. ISSN 0033295X. doi: 10.1037/REV0000070.
- [79] R. D.S. Raizada and S. Grossberg. Context-sensitive binding by the laminar circuits of V1 and V2: A unified model of perceptual grouping, attention, and orientation contrast. *Visual Cognition*, 8(3-5):431–466, 2001. ISSN 13506285. doi: 10.1080/13506280143000070.
- [80] James R. Pomerantz, Lawrence C. Sager, and Robert J. Stoeber. Perception of wholes and of their component parts: Some configural superiority effects. *Journal of Experimental Psychology: Human Perception and Performance*, 3(3):422–435, 1977. ISSN 00961523. doi: 10.1037/0096-1523.3.3.422.
- [81] D. D. Hoffman and W. A. Richards. Parts of recognition. *Cognition*, 18(1-3):65–96, December 1984. ISSN 0010-0277. doi: 10.1016/0010-0277(84)90022-2.
- [82] Yaoda Xu and Manish Singh. Early computation of part structure: Evidence from visual search. *Perception & psychophysics*, 64(7):1039–1054, 2002. ISSN 0031-5117. doi: 10.3758/BF03194755.
- [83] Goker Erdogan and Robert A. Jacobs. Visual shape perception as Bayesian inference of 3D object-centered shape representations. *Psychological Review*, 124(6):740–761, 2017. ISSN 0033295X. doi: 10.1037/rev0000086.
- [84] Zili Liu, David C. Knill, and Daniel Kersten. Object classification for human and ideal observers. *Vision Research*, 35(4):549–568, 1995. ISSN 00426989. doi: 10.1016/0042-6989(94)00150-K.

- [85] Ken Nakayama, Zijiang J. He, and Shinsuke Shimojo. Visual Surface Representation: A Critical Link between Lower-Level and Higher-Level Vision. *An Invitation to Cognitive Science*, October 1995. doi: 10.7551/MITPRESS/3965.003.0004.
- [86] Greet Kayaert, Irving Biederman, and Rufin Vogels. Shape Tuning in Macaque Inferior Temporal Cortex. *Journal of Neuroscience*, 23(7):3016–3027, April 2003. ISSN 0270-6474. doi: 10.1523/JNEUROSCI.23-07-03016.2003.
- [87] Jonas Kubilius, Johan Wagemans, and Hans P. Op de Beeck. Emergence of perceptual Gestalts in the human visual cortex: The case of the configural-superiority effect. *Psychological science*, 22(10):1296–1303, 2011. ISSN 1467-9280. doi: 10.1177/0956797611417000.
- [88] A. Gomez-Villa, A. Martín, J. Vazquez-Corral, M. Bertalmío, and J. Malo. Color illusions also deceive CNNs for low-level vision tasks: Analysis and implications. *Vision Research*, 176:156–174, November 2020. ISSN 0042-6989. doi: 10.1016/J.VISRES.2020.07.010.
- [89] Valeria Anna Sovrano, Osvaldo da Pos, and Liliana Albertazzi. The Müller-Lyer illusion in the teleost fish *Xenotoca eiseni*. *Animal cognition*, 19(1):123–132, January 2016. ISSN 1435-9456. doi: 10.1007/S10071-015-0917-6.
- [90] Hongtao Zhang, Zhen Li, and Shinichi Yoshida. Müller-Lyer illusion is Replicated by Higher Layer of Pre-trained Deep Neural Network for Object Recognition. Müller-Lyer illusion is Replicated by Higher Layer of Pre-trained Deep Neural Network for Object Recognition. In *The 10th International Symposium on Computational Intelligence and Industrial Applications (ISCIIA2022, Zhang2022mullerlyer, 2022*.
- [91] Dongjun He, Ce Mo, Yizhou Wang, and Fang Fang. Position shifts of fMRI-based population receptive fields in human visual cortex induced by Ponzo illusion. *Experimental brain research*, 233(12):3535–3541, December 2015. ISSN 1432-1106. doi: 10.1007/S00221-015-4425-3.
- [92] Irene Sperandio, Philippe A. Chouinard, and Melvyn A. Goodale. Retinotopic activity in V1 reflects the perceived and not the retinal size of an afterimage. *Nature neuroscience*, 15(4):540–542, April 2012. ISSN 1546-1726. doi: 10.1038/NN.3069.
- [93] Juan Chen, Irene Sperandio, Molly J. Henry, and Melvyn A. Goodale. Changing the Real Viewing Distance Reveals the Temporal Evolution of Size Constancy in Visual Cortex. *Current Biology*, 29(13):2237–2243.e4, July 2019. ISSN 0960-9822. doi: 10.1016/J.CUB.2019.05.069.
- [94] Robert L. Whitwell, Mehul A. Garach, Melvyn A. Goodale, and Irene Sperandio. Looking at the Ebbinghaus illusion: Differences in neurocomputational requirements, not gaze-mediated attention, explain a classic perception-action dissociation. *Philosophical Transactions of the Royal Society B: Biological Sciences*, 378(1869):20210459, December 2022. doi: 10.1098/rstb.2021.0459.
- [95] V. H. Franz, F. Scharnowski, and K. R. Gegenfurtner. Illusion effects on grasping are temporally constant not dynamic. *Journal of experimental psychology. Human perception and performance*, 31(6):1359–1378, December 2005. ISSN 0096-1523. doi: 10.1037/0096-1523.31.6.1359.
- [96] Astrid Busch and Hermann J. Müller. The Ebbinghaus illusion modulates visual search for size-defined targets: Evidence for preattentive processing of apparent object size. *Perception & Psychophysics*, 66(3):475–495, April 2004. ISSN 1532-5962. doi: 10.3758/BF03194895.
- [97] Einat Rashal, Aline F. Cretienoud, and Michael H. Herzog. Perceptual grouping leads to objecthood effects in the Ebbinghaus illusion. *Journal of Vision*, 20(8):11–11, August 2020. ISSN 1534-7362. doi: 10.1167/JOV.20.8.11.
- [98] Irvin Rock. *An Introduction to Perception*. Macmillan, New York, NY, 1975. ISBN 978-0-02-402490-9.
- [99] Christian Agrillo, Michael J. Beran, and Audrey E. Parrish. Exploring the Jastrow Illusion in Humans ( *Homo sapiens*), Rhesus Monkeys ( *Macaca mulatta*), and Capuchin Monkeys ( *Sapajus apella*). *Perception*, 48(5): 367–385, May 2019. ISSN 1468-4233. doi: 10.1177/0301006619838181.
- [100] Aviad Ozana and Tzvi Ganel. A double dissociation between action and perception in bimanual grasping: Evidence from the Ponzo and the Wundt–Jastrow illusions. *Scientific Reports 2020 10:1*, 10(1):1–10, September 2020. ISSN 2045-2322. doi: 10.1038/s41598-020-71734-z.
- [101] Colin W.G. Clifford. The tilt illusion: Phenomenology and functional implications. *Vision Research*, 104:3–11, November 2014. ISSN 18785646. doi: 10.1016/j.visres.2014.06.009.

- [102] Thomas Serre, Drew Linsley, and Junkyung Kim. What is the function of the orientation-tilt illusion? *Journal of Vision*, 20(11):868, October 2020. ISSN 1534-7362. doi: 10.1167/jov.20.11.868.
- [103] Chen Song and Geraint Rees. Intra-hemispheric integration underlies perception of tilt illusion. *NeuroImage*, 175:80–90, July 2018. ISSN 10959572. doi: 10.1016/j.neuroimage.2018.03.073.
- [104] Drew Linsley, Junkyung Kim, Alekh Ashok, and Thomas Serre. Recurrent neural circuits for contour detection. In *International Conference on Learning Representations*, 2020. URL <https://openreview.net/forum?id=H1gB4RVKvB>.
- [105] Gerald Westheimer. Simultaneous orientation contrast for lines in the human fovea. *Vision Research*, 30(11):1913–1921, January 1990. ISSN 00426989. doi: 10.1016/0042-6989(90)90167-J.
- [106] S. P. MacEvoy and M. A. Paradiso. Lightness constancy in primary visual cortex. *Proceedings of the National Academy of Sciences of the United States of America*, 98(15):8827–8831, July 2001. ISSN 00278424. doi: 10.1073/PNAS.161280398/ASSET/5C272BB0-31B1-4A16-A83F-18033A56DFDD/ASSETS/GRAPHIC/PQ1612803004.JPEG.
- [107] Alban Flachot, Arash Akbarinia, Heiko H. Schütt, Roland W. Fleming, Felix A. Wichmann, and Karl R. Gegenfurtner. Deep neural models for color classification and color constancy. *Journal of Vision*, 22(4):17–17, March 2022. ISSN 1534-7362. doi: 10.1167/JOV.22.4.17.
- [108] Stephen Grossberg. The quantized geometry of visual space: The coherent computation of depth, form, and lightness. *Behavioral and Brain Sciences*, 6(4):625–657, 1983. ISSN 1469-1825. doi: 10.1017/S0140525X00017763.
- [109] Evelin Bertin and Ramesh S. Bhatt. The Thatcher illusion and face processing in infancy. *Developmental Science*, 7(4):431–436, 2004. ISSN 1467-7687. doi: 10.1111/j.1467-7687.2004.00363.x.
- [110] Christoph D. Dahl, Nikos K. Logothetis, Heinrich H. Bühlhoff, and Christian Wallraven. The Thatcher illusion in humans and monkeys. *Proceedings of the Royal Society B: Biological Sciences*, 277(1696):2973–2981, October 2010. ISSN 0962-8452, 1471-2954. doi: 10.1098/rspb.2010.0438.
- [111] Irving Biederman and Ginny Ju. Surface versus edge-based determinants of visual recognition. *Cognitive Psychology*, 20(1):38–64, January 1988. ISSN 00100285. doi: 10.1016/0010-0285(88)90024-2.
- [112] Robert Geirhos, Patricia Rubisch, Claudio Michaelis, Matthias Bethge, Felix A. Wichmann, and Wieland Brendel. Imagenet-trained CNNs are biased towards texture; increasing shape bias improves accuracy and robustness. In *International Conference on Learning Representations*, 2019. URL <https://openreview.net/forum?id=Bygh9j09KX>.
- [113] Mostafa Dehghani, Josip Djolonga, Basil Mustafa, Piotr Padlewski, Jonathan Heek, Justin Gilmer, Andreas Peter Steiner, Mathilde Caron, Robert Geirhos, Ibrahim Alabdulmohsin, Rodolphe Jenatton, Lucas Beyer, Michael Tschannen, Anurag Arnab, Xiao Wang, Carlos Riquelme Ruiz, Matthias Minderer, Joan Puigcerver, Utku Evci, Manoj Kumar, Sjoerd Van Steenkiste, Gamaleldin Fathy Elsayed, Aravindh Mahendran, Fisher Yu, Avital Oliver, Fantine Huot, Jasmijn Bastings, Mark Collier, Alexey A. Gritsenko, Vignesh Birodkar, Cristina Nader Vasconcelos, Yi Tay, Thomas Mensink, Alexander Kolesnikov, Filip Pavetic, Dustin Tran, Thomas Kipf, Mario Lucic, Xiaohua Zhai, Daniel Keysers, Jeremiah J. Harmsen, and Neil Houlsby. Scaling vision transformers to 22 billion parameters. In Andreas Krause, Emma Brunskill, Kyunghyun Cho, Barbara Engelhardt, Sivan Sabato, and Jonathan Scarlett, editors, *Proceedings of the 40th International Conference on Machine Learning*, volume 202 of *Proceedings of Machine Learning Research*, pages 7480–7512. PMLR, 23–29 Jul 2023. URL <https://proceedings.mlr.press/v202/dehghani23a.html>.
- [114] Jacob Beck, K. Prazdny, and Aziel Rosenfeld. A Theory of Textural Segmentation. In *Human and Machine Vision*, pages 1–38. Elsevier, 1983. ISBN 978-0-12-084320-6. doi: 10.1016/B978-0-12-084320-6.50007-4.
- [115] Kirsten R. Pantou, David R. Badcock, and Johanna C. Badcock. A Metaanalysis of Perceptual Organization in Schizophrenia, Schizotypy, and Other High-Risk Groups Based on Variants of the Embedded Figures Task. *Frontiers in Psychology*, 7, 2016. ISSN 1664-1078.
- [116] Katrien Torfs, Kathleen Vancleef, Christophe Lafosse, Johan Wagemans, and Lee De-Wit. The Leuven Perceptual Organization Screening Test (L-POST), an online test to assess mid-level visual perception. *Behavior Research Methods*, 46(2):472–487, November 2014. ISSN 15543528. doi: 10.3758/S13428-013-0382-6/FIGURES/18.

- 
- [117] Ryan Blything, Valerio Biscione, and Jeffrey Bowers. A case for robust translation tolerance in humans and CNNs. A commentary on Han et al. *arXiv preprint arXiv: 2012.05950*, December 2020.
- [118] Diederik P Kingma. Adam: A method for stochastic optimization. *arXiv preprint arXiv:1412.6980*, 2014.
- [119] Zhaoyang Pang, Callum Biggs O’May, Bhavin Choksi, and Rufin VanRullen. Predictive coding feedback results in perceived illusory contours in a recurrent neural network. *Neural Networks*, 144:164–175, 2021. ISSN 0893-6080. doi: <https://doi.org/10.1016/j.neunet.2021.08.024>. URL <https://www.sciencedirect.com/science/article/pii/S0893608021003373>.
- [120] Matthew D. Zeiler and Rob Fergus. Visualizing and understanding convolutional networks. In *Lecture Notes in Computer Science (Including Subseries Lecture Notes in Artificial Intelligence and Lecture Notes in Bioinformatics)*, volume 8689 LNCS, pages 818–833. Springer Verlag, 2014. ISBN 978-3-319-10589-5. doi: 10.1007/978-3-319-10590-1\_53.
- [121] Ting Chen, Simon Kornblith, Mohammad Norouzi, and Geoffrey Hinton. A simple framework for contrastive learning of visual representations. In *International conference on machine learning*, pages 1597–1607. PMLR, 2020.
- [122] Gene Tangtartharakul and Katherine R Storrs. Visual language models show widespread visual deficits on neuropsychological tests. *arXiv preprint arXiv:2504.10786*, 2025.

## Supplementary Material for MindSet: Vision

### A Experimental Stimuli

Below we provide more details about the various conditions included in MindSet: Vision and their relevance to understanding human vision. We also highlight the most important parameters for each dataset. For a complete list, refer to the generated HTML page <sup>2</sup> which additionally contains several samples for each condition and each dataset when generated using default parameters. Examples of stimuli from all 30 Experiments are presented in Figure A.1.

#### A.1 Low and Mid-level vision

There is no sharp dividing line between early and middle visual processing, but early vision extracts low level feature information (i.e., color and luminance contrasts, the orientation of bar and edge segments, and contour segments) from the retinal image. By contrast, mid level vision encodes more abstract aspects of shape, such as surfaces and parts of objects, in an increasingly viewpoint invariant manner. This is where representations of 2D and 3D shapes, material properties, and coherence of the substances and surfaces in the world are computed. That is, mid-level vision builds representations of the distal world from the proximal stimulus. This is an ill-posed problem, and accordingly, various heuristics (such as Gestalt perceptual grouping cues) are employed to provide the best estimate of the distal world. Illusions are striking examples of failures to correctly encode the distal world from the proximal stimulus. The experiments we include in MindSet: Vision largely focus on mid-level vision.

##### A.1.1 Weber Law

**Psychological Significance.** The Weber Law (or Weber-Fechner Law) quantifies the psychophysical relation between changes in the world and changes in perception. The law states that the minimum physical change of a stimulus on some dimension (e.g., its size) that is perceptible to an observer is a constant ratio of the original stimulus value on this dimension. For example, it is easy to distinguish between line lengths of 1 and 2 cm, but difficult to distinguish between lines of length 100 and 101 cm, despite the fixed difference in length (1 cm). To make the latter distinction equally salient, the two stimuli should be 100 and 200 cm (a fixed ratio of 2). Although Weber’s Law breaks down at extreme values, this relationship applies to a wide range of dimensions, from weight, length, size, brightness, and even numbers. Weber’s Law reflects the more general observation that perception is often based on relative rather than absolute encoding of stimulus dimensions. Importantly, Weber’s Law is often manifest in early visual areas [72], and indeed, in some cases, at the level of the retina [73–75].

[39] reported that the convolutional DNN VGG-16 showed a human-like Weber Law effect when encoding line-lengths. However, the authors only observed Weber’s Law for line lengths in the late convolutional layers of the network, did not assess whether discrimination was a constant ratio of the original stimulus (they employed a weaker test), and failed to observe a reliable effect for image intensity.

**Dataset.** Images in this dataset are composed of a simple horizontal white line with varying length and brightness values. Configurable parameters include line width, min/max values for length and brightness. To assess DNNs sensitivity to Weber’s Law, a similarity judgment analysis assesses whether the relative change in the perception of these stimuli (as measured by the level of unit activation in the inner layers of a pre-trained DNN) adheres to a logarithmic relationship with the stimulus strength (e.g. line length).

##### A.1.2 Crowding / Uncrowding

**Psychological Significance.** Our ability to identify objects is impaired by the presence of nearby objects and shapes, a phenomenon called crowding. At the same time, in some conditions, the inclusion of additional surrounding objects makes the identification of the target easier, a phenomenon called uncrowding. This is illustrated in Figure A.2, in which participants are asked to perform a vernier discrimination task by deciding whether the top vertical line from a pair of vertical lines is shifted to the left or right. When these lines are surrounded by a square rather than presented by themselves performance is impaired. However, the inclusion of additional squares dramatically improves performance. This is thought to reflect a Gestalt process in which the squares are grouped together and then processed separately from the vernier [76]. Standard DNNs are unable to explain uncrowding [77, 78], but the DNNs inspired by the LAMINART model of Grossberg and colleagues [79] designed to support grouping processes can capture some aspects of uncrowding.

---

<sup>2</sup>MindSet: Vision summary HTML

**Dataset.** Based on [77], with code adapted with authors’ permission. Images are composed of a ‘vernier’ stimulus (two parallel line segments with some offset) placed either inside or outside a set of random flankers (squares, circles, hexagons, octagons, stars, diamonds). Each configuration has from 1 to 7 columns and from 1 to 3 rows of flankers with a variety of same/different shape patterns used. The vernier can be left/right oriented. The suggested method for this dataset [as per 77] consists of attaching a decoder at several stages of a pre-trained DNN. The decoder is trained and tested on a classification task to discriminate between left/right types of vernier but, significantly, during training, the vernier and the flankers were non-overlapping, whereas during test, the vernier was often placed inside one of the shapes, allowing the measuring of (un)crowding effect through change in classification accuracy across test conditions. A model with human-like visual characteristics should match human perception with regards to both crowding and uncrowding effects, following the pattern in [30, 77]. Users can specify whether the size of the flankers varies or is fixed across samples.

### A.1.3 Emergent features

**Psychological Significance.** Emergent features provide a compelling example of “the whole is different than the sum of its parts”. Pomerantz and colleagues [27, 80] relied on a simple visual search paradigm where participants were asked to identify a target amongst foils. They devised several different types of target and foil stimuli, but the simplest were composed of dot patterns as depicted below. Participants viewed a set of 4 panels, each of which contained a single dot. Three of these panels were identical (dots were in the same location) and one outlier panel (where the dot was in a different location). The task was to identify the outlier panel as quickly as possible. In the single dot condition, the outlier was simply the panel with a dot in a unique position. In the critical emergent feature condition(s), a dot (or more) was added to the single dot images as context. The context dot(s) was in the same location in all panels. Because these added dot(s) were identical in all four panels, there were no new features that could be used to facilitate the identification of the outlier other than configural “emergent” features. For example, in the top row of Figure A.3, the extra dot (depicted in the middle column) produces the emergent feature of “orientation”, and in the bottom row, the extra dot produces the emergent feature of proximity. The critical finding was that participants could identify the location of the outlier panel more quickly in the emergent compared to the baseline condition. That is, the “whole” was more discriminable than the sum of its parts.

[29] carried out a series of studies assessing whether DNNs were sensitive to a range of emergent features that facilitated human performance, including testing DNNs on the dot stimuli illustrated in Figure A.3. It was observed that DNNs did show some sensitivity to some of the emergent features, but only at the later layers of the network. This is problematic given that these emergent features are thought to be computed relatively early in the visual system, such that they support rapid “pop out” search.

**Dataset.** Adapted from [29]. The dataset consisted of sets of paired images. Each set includes four conditions: a base condition (single dots), and composite conditions (orientation, proximity, and linearity). The ‘single dots’ condition consists of paired images in which each image contains a single dot placed at a different location. In the composite conditions, one or more dots are added to both images of the base condition, in the same locations, in such a way that it would elicit different emergent properties when combined with the original single dots. In the orientation and proximity conditions, the added dot results in different orientation/proximity features. In the linearity condition (generated by adding a dot to the orientation condition), the added dot would either be placed on a straight line with the other two dots or on a different path. Each dot was constrained to be located at a distance of at least 20 pixels from one another, and 40 pixels from the border. By computing the difference in similarity scores between each composite condition and the base condition, we can compute how much each emergent feature impairs/facilitates distinction of the additional dots. For example, if the average ‘orientation’ pair is found to be easier to distinguish (through a similarity analysis of the internal activations of the network) than the pairs from the ‘single dot’ condition, then we can infer that the network is sensitive to orientation (as the additional dot in the orientation condition was not-diagnostic, e.g. the same for both images in each pair). The same comparison with the ‘single dot’ pairs can be performed for the proximity and linearity conditions. The overall pattern of similarity scores should match human results, in which the highest effect is obtained through the feature of proximity, followed by linearity, and then orientation [27, 29].

### A.1.4 Decomposition

**Psychological Significance.** The visual system represents objects in terms of their parts, separating regions at points of deep concavity [81]. Perceptually, searching for an object broken into its natural parts among a set of unsegmented versions of the same object is significantly more challenging than locating the same object when it is segmented at points that do not correspond to its natural divisions. In other words, a segmentation at natural points preserves the basic parts which make up the object and therefore make the segmented version more similar to the uncut object when compared to an ‘unnatural’ segmentation. There is good evidence that this occurs relatively early in visual processing [82]. To assess

whether DNNs encode objects into parts in a similar manner, [39] compared the internal representations of a base object composed of two parts to two segmentations of the object, one natural and one unnatural. The assumption is that a natural segmentation of the image will be encoded in a more similar way to the whole object (the segmented images maintain the integrity of parts that compose the complete object). However, they reported that the VGG-16 did not show this pattern, suggesting that DNNs do not encode objects by their parts, or at least, not in a way similar to humans.

**Dataset.** The dataset consists of a variation of the images used in [39]: instead of a single object composed of two parts, we used two objects joined at a single point of contact. There are three ‘split’ conditions and two ‘familiarity’ conditions. The ‘split’ conditions are: ‘no split’ in which two parts are touching at one point but not overlapping; ‘natural split’, in which two parts are separated; ‘unnatural split’ in which the two parts are touching each other as in the ‘no split’ condition, but one of the parts is ‘cut’ and separated from the rest. The items are silhouettes uniformly coloured on a uniform background, and they can be either familiar or unfamiliar shapes. The familiar shapes consist of the following objects: circle, square, rectangle, triangle, heptagon, and a 50-degree arc segment; the unfamiliar shapes consist of blob-like objects. Within each familiar/unfamiliar condition, all possible combinations of two shapes are used (e.g. a triangle with a rectangle). Configuration parameters include the distance between pieces in the ‘unnatural split’ and ‘natural split’ conditions, the colour of items, and the number of different blob-like objects to use for the unfamiliar condition. Following the test from [39], similarity judgments between pairs composed of base samples and natural/unnatural splits can be computed for an ImageNet pre-trained network. To match human perception, the natural split samples should have internal representations that are closer to the base samples than the unnatural split samples. This should apply regardless of whether the shapes are familiar or unfamiliar.

### A.1.5 Encoding relations between object parts

**Psychological Significance.** Humans not only encode objects in terms of their parts, but also the relations between parts which are essential for object recognition [31]. Early evidence for this was reported by [36] who trained participants to identify a small set of artificial stimuli in which they could easily manipulate relations between parts. Two types of changes were introduced to create foils for the base stimuli. First, a coordinate change in which relations between parts were maintained but the position of a part of the object was changed. And second, a relational change in which there was a categorical change in relations between object parts. They reported that participants were much more likely to mistake foil objects for the base object when the relations between object parts were maintained than when the relations changed (coordinate vs relational change in Figure A.5). By contrast, [35] showed that two standard convolutional networks are completely insensitive to these relational features, treating Relational and Coordinate foils equally similar to the Basis objects.

**Dataset.** We recreated images originally contained in [36], Experiment 5, using white strokes on a uniform background. To compare to human perception, similarity judgments can be computed from pre-trained DNNs by sequentially inputting pairs of images composed of a base shape and either their corresponding coordinate or relational change. A pattern that mirrors human perception would result in greater similarity between the base shapes and their coordinate modifications foils as opposed to their relational change foils.

### A.1.6 Encoding of 3D shapes

**Psychological Significance.** The human visual system builds 3D representations of images for the sake of object recognition [83, 84], and some perceptual illusions of size, such as the Ponzo illusion described below, are thought to be a by-product of computing depth information. By contrast, there is little evidence that DNNs infer 3D structure from the 2D images they process. For example, [39] tested VGG-16 on three pairs of objects developed by [40]: a pair of objects composed of three segmented lines (base pair in Figure A.6) are transformed in two different ways (V1 and V2), each time adding the same configuration to both elements of the base pair. Humans were assessed in how quickly they could discriminate the two V1 images and the two V2 images. Discrimination was highly improved for the V2 pair, but not for the V1 pair, most likely the result of enhanced 3D cues in the V2 stimuli.

In contrast, [39] obtained no evidence that VGG-16 was better at discriminating the base pair, suggesting a failure to encode their 3D structure.

**Dataset.** We recreated stimuli appearing in [40], using white strokes on a uniform background. Using the similarity judgment method on pre-trained DNNs, a perception akin to humans would result in a significantly lower similarity for the V2 pair compared to both the base and V1 images.

### A.1.7 Amodal completion

**Psychological Significance:** The visual system needs to identify partly occluded objects in the 3D world. A key part of the solution for humans is an amodal completion process in which a surface representation of the occluded object

is completed behind the occluder. This process is called amodal because the visual system builds complete surface forms of occluded objects without generating a visible experience of the missing shape. Amodal completion occurs early in the visual system, perhaps as early as V1 [37]. Various compelling perceptual effects are associated with amodal completion [for a review see 85]. Here we include the materials from [38] who showed that humans quickly and automatically encode the shape of partially occluded objects in a visual search task.

Amongst the various conditions in their experiments, two illustrate the point most clearly. In the 'Target - Notched square' and 'Target - notched circle' conditions, participants searched for a notched black square or notched white circle, respectively, among full black square and white circle distractors. None of the objects overlapped in this condition. In the 'Occlusion' condition participants were again searching for notched squares and circles, but in this case notched squares and circles touched to give the impression of occlusion. Search was significantly faster in the 'Notched' condition when compared to the 'Occlusion' condition. This is because in the 'Occlusion' condition the notched squares were perceived as full squares occluded by white disks due to amodal completion. This made the notched black squares much more difficult to find among full black squares. The same was true for the notched white circles in the occlusion condition. This pattern of results suggests that the notched square in the 'Occlusion' condition was encoded as a square early in visual processing (fast visual search is typically characterized as pre-attentive). [39] reported that the DNN VGG-16 network pre-trained on ImageNet failed to show any evidence for amodal completion with these stimuli.

**Dataset.** We generated samples that look like the stimuli used in [38]. We generated samples for the distractors ('unoccluded'), 'occlusion', and 'notched' conditions, with either the square occluding the circle or vice versa. The occluding shape is placed at a variety of degrees from the occluded shape. Each occluded image has a corresponding notched image (that is, using the same shape configurations) so that they can be directly compared. The unoccluded condition is generated by using a non-occluded sample in which the occluding shape is moved radially away from the occluded shape, maintaining the same orientation.

To align with human similarity judgments as measured in [38], a DNN should yield internal activations that result in higher similarity scores for distractor (unoccluded) versus occluded samples (where amodal completion generates representations of the full shape of the notched stimuli), compared to those for (distractor) unoccluded versus notched samples.

### A.1.8 Non-accidental and Metric Properties for Geons and line stimuli

**Psychological Significance:** Human object recognition is highly sensitive to non-accidental properties (NAPs) of an object, that is, visual features that are invariant over rotations in depth. NAPs are hypothesized to be critical for representing object parts such as Geons [31]. For example, curvature (as opposed to a straight line) is a NAP because a curved object in the 3D world will project a curved image on a 2D retina when viewed from most orientations apart from rare "accidental" viewpoints, as when a curve projects a straight contour. NAPs are distinguished from metric properties (MP), features of objects that change continuously with variations over depth orientation when projected on the retina. For example, a curved object in the world will project different degrees of curvature on the retina depending on its orientation to the viewer. A variety of research highlights how human vision is more sensitive to changes in images that alter NAPs (e.g., a change from a curve to straight line) compared to MPs (e.g., changes in degree of curvature) [31]. [34] provided evidence that several DNNs are also more sensitive to image manipulations that alter NAPs, although the effects were most pronounced in later layers of the networks whereas sensitivity to NAP is thought to occur relatively early in human visual processing to encode object parts.

**Datasets.** We have included images of both **2D line segments** based on [34], and **3D Geon stimuli** originally used in [86] to assess the degree in which DNNs are sensitive to NAP vs MP changes. In the case of the Geon stimuli, we have provided a version with shade [as in 87], a version in which no shades are present and the outline is highlighted, and a version in which only the silhouettes are shown, as one concern with the shaded version is that the similarity judgements produced by DNNs may reflect differences in shades as opposed to shape. For each Geon or line segment, a feature dimension (such as the curvature of a Geon) is altered from a singular value (e.g. straight contour with 0 curvature) to two different values (e.g. slightly curved or very curved). The 'reference' condition includes items with the intermediate feature value; in this example, the slightly curved geon. The 'MP change' condition consists of items with a greater non-singular value; in this case, the greater curvature geon. Finally, the 'NAP change' condition includes items with the singular value; the straight contour geon from this example. A human-like similarity judgment would correspond to higher similarity between the reference object to the MP variants than the NAP variants (that is, NAP changes are easier to discriminate). [34] provides a more detailed description of human performance through reaction times that can be directly compared to similarity judgments in DNNs (where higher reaction times correspond to lower similarity).

## A.2 Visual Illusions

There is now a growing number of articles exploring various illusions in various different types of DNNs trained in different ways. Some of these highlight similarities with human perception [e.g., 53–55] while others report mixed or discrepant results [e.g., 23, 56, 57, 88]. For a review of various findings see [18]. The conditions in which DNNs ‘experience’ human-like illusions may provide insights into why humans experience these phenomena. For instance, [56] found that various brightness and color illusions can be induced in CNNs trained for image denoising, image deblurring, and computational color constancy. They argue that these illusions are a byproduct of biological processes designed to improve efficiency of low-level visual processes. In addition, [54] found that unsupervised (as opposed to supervised) learning led DNNs to factorize images into encoding of reflectance and illumination that resulted in a human-like perceptual illusion of gloss. Here we consider several classic size, lightness, and orientation illusions. For most of the Visual Illusions Datasets, we provide both an “illusory” condition and a corresponding “non-illusory” condition. The non-illusory condition contains the same basic elements as the illusory one, but they are arranged in such a way that the illusion is not elicited. Both conditions feature procedurally generated images. In the illusory conditions, the stimuli are systematically varied to maintain the presence of the illusion. For example, in the Ponzo illusion dataset, we manipulate factors such as the number of horizontal “railway” lines, the degree of convergence of the vertical lines, and the length of each line. However, we carefully constrain these variations to ensure that the illusion remains effective. We encourage future researchers who wish to modify our scripts or use non-default parameters to regenerate the datasets to verify that the illusory stimuli continue to produce the intended perceptual effects.

### A.2.1 Müller-Lyer illusion

**Psychological Significance.** The Müller-Lyer illusion is perhaps the most famous of all illusions. There is no agreed-upon explanation of the effect but the fact that it is observed across species, including fish [89], suggests that it reflects something basic about the architecture of the visual system rather than the training environment. [57] reported that VGG-19 showed the illusion (to a rough approximation), although they only reported the effect at the final stage of the network. A similar result was reported by [90] who reported more robust effects in the higher levels of VGG-19 and ResNet-101.

**Dataset.** The Müller-Lyer illusion stimuli were generated in one of two ‘illusory’ configurations (with inward or outward ‘fins’) or in a ‘scrambled’ configuration. In the latter, the fins are arranged randomly in the canvas, separated from the line segment. In all three conditions, we vary the line length, the position of the line, and the angle of the fins. A method to test whether a DNN is susceptible to this illusion involves training a set of decoders to predict the line length in the scrambled condition set. These decoders are then tested on the illusory conditions. A human-like response would be evidenced by a consistent pattern of both overestimating the line length in the outward illusory condition and underestimating it in the inward illusory condition. Additionally, the illusory effect should be larger for more acute fin angles.

### A.2.2 Ponzo illusion

**Psychological Significance.** In this classic illusion, two identical horizontal lines cross a pair of converging lines, a configuration similar to railway tracks. In this configuration, the top line looks longer. The standard explanation is that the visual system assumes that the converging lines are receding in depth and that the upper horizontal line is further away. Given that the two lines project the same length on the retina, the visual system assumes that the upper line must be longer. That is, the illusion is a by-product of the visual system attempting to compute size constancy. Interestingly, there is good evidence that the Ponzo illusion [91], and related size illusions [92], alter the activation in V1, although this may reflect top-down activation from higher-level visual areas [93]. [57] failed to observe a Ponzo effect in VGG-19.

**Dataset.** Two target lines (red and blue) are placed across a railway track pattern. In the illusory condition, the target lines have the same length (varying across samples). In the scrambled condition, the target lines have different length, are still placed horizontally one on top of the other, but all the other segments are randomly placed across the canvas. We include a third condition in which the railway track pattern is used with target lines which differ in length. The railway track pattern for the illusory and different lengths conditions is composed of converging segments (with a varying degree of convergence), and horizontal segments (randomly placed at different horizontal positions). For all three conditions, the user can specify the number of horizontal segments to use.

The suggested way to test whether DNNs perceive the Ponzo Illusion consists of training a set of decoders on the scrambled condition, to predict either the length of the target lines or a function of the length (for example, the difference between the top and the bottom line lengths). Then the decoders can be tested on the illusory condition. The different lengths condition could be used as a further way of analysing the decoders response. To match human perception, a

decoder should overestimate the length of the top target line (or underestimate the length of the bottom line, or output a positive difference in top minus bottom line length, depending on the training setup) in the illusory condition (where the two target lines have the same length).

### A.2.3 Ebbinghaus (or Titchener) illusion.

**Psychological Significance:** In this classic illusion, the perceived size of a central circle is altered by the size of surrounding circles. There is evidence that the illusion distorts the perception of size but not action (45, 94; but see 95) and there is evidence that this illusion is mediated by relatively low-level (preattentive) vision [96]. Again, there are different explanations for the phenomena [97]. [57] failed to observe this effect in VGG-19.

**Dataset.** A red target circle is surrounded by a fixed number of white circles (flankers) on a uniform background. In the two illusory conditions ('big' and 'small' flankers) the flankers surround the target circle, and they all have the same size within each sample. In the scrambled condition the target circle is placed in the center, but white circles with random sizes are randomly placed on the canvas. Across illusory samples, we varied the radii of the flankers, the radius of the target circle, the displacement of the flankers around the target. To measure illusory effects in DNNs, decoders can be trained on estimating the circle size or radius in the scrambled condition, and tested on the big/small flankers condition. Human-like perception should induce overestimating in the small flankers condition and under-estimating in the big flankers condition (see example in Figure D.1).

### A.2.4 Jastrow Illusion

**Psychological Significance:** In the Jastrow Illusion [46], two identical-sized curved segments are perceived as different sizes when one is placed above the other in certain configurations. There are multiple explanations for the phenomenon, but perhaps the simplest explanation is that it is a form of a contrast effect. The length of the concave edge of the upper object in a Jastrow configuration is much shorter than the convex edge of the bottom object, and this contrast drives the perception of size when the edges are closely aligned [98]. Rhesus monkeys do not appear to be affected [99], nor do humans when assessed on grasping behavior [100]. As far as we are aware, no one has reported whether DNNs show a similar pattern.

**Dataset.** We used a red and a blue arc shape, either one on top of the other at the centre of the canvas ('illusory' and 'different lengths' conditions) or randomly placed in the canvas with a random orientation ('scrambled' condition). In the scrambled and different lengths conditions the two shapes have different sizes. The size is the same (thus eliciting the illusion) in the illusory condition. To estimate DNNs susceptibility to the illusion the same approach as the Ponzo Illusion can be used.

### A.2.5 Tilt illusion

**Psychological Significance:** In the tilt illusion, a central grating's orientation is perceived as being repulsed from or attracted to the orientation of a surrounding grating. A wide variety of mechanistic accounts of the illusion have been proposed [for a review see 101], and it is argued to be an adaptive feature rather than a bug of a visual system optimized for contour detection [102]. There is evidence that the illusion reflects processes in V1 [103]. [104] reported that a recurrent DNN optimized for contour detection produces a tilt illusion.

**Dataset.** We provide one illusory condition, in which an oriented grating pattern is presented within a circular mask ('center grating') and a differently oriented grating is placed as the background ('context' grating); and two non-illusory conditions: one in which the background is uniformly colored and only a center mask contains the oriented grating pattern; and vice versa. The samples are varied in their orientation and spatial frequency of the gratings, and in the size of the central grating. Our suggested approach to test whether a DNN perceives the tilt illusion is to train a decoder to estimate the orientation of the center grating, and test it on the illusory condition to check whether the presence of a context affects performance. In particular, the decoder should present the largest repulsive bias at around  $20^\circ$  and an attractive bias at around  $70^\circ$ - $80^\circ$ . Plus, the attractive effect should be much smaller than the repelling effect, and larger for matching center-surround gratings spatial frequencies. [105].

### A.2.6 Lightness Illusions

Lightness refers to our perception of the reflective surface of an object (a stable property of an object) whereas brightness is a measure of the amount of light reflected from an object, something that is affected by both reflectance as well as the lighting source. We include two famous illusions related to lightness: the Lightness Contrast Illusion and the Adelson Checker Shadow Illusion. However, to facilitate testing for these and other lightness-related effects, we created an additional dataset called '**Grayscale shapes**'. The purpose of this dataset is not to elicit any illusion in humans or in

DNNs but to train a network (or, with our suggested method, a decoder attached to a network) to output the grayscale value of a target pixel.

**Grayscale shapes Dataset.** Each image is composed of 20 overlapping items amongst the following types of shapes (circle, circle sector, circle segment, ellipse, rectangle with straight and rounded corners, heptagon, irregular polygon composed of a random number of edges from 3 to 10). Position, dimension, orientation, and grayscale colour value are randomized for each shape. We place 20 items to be sure that most space in the canvas is filled by an item, but that only a few of them are fully visible. This results in a chaotic canvas with many different shapes with varying grayscale colours but with coherent patterns (as opposed to, for example, having each pixel of a different random grayscale value). In order to target a specific pixel to be predicted by the decoder, a small white vertical arrow (the ‘marker’) of fixed size is placed randomly on the canvas. The arrow points to the pixel whose value can be used for prediction. Notice that while the images are commonly normalized from -1 to 1 before being fed into the network, the targeted pixel value to predict is in the 0-255 range. Once a trained decoder reaches the desired level of accuracy, it can be tested on other configurations by simply adding the white arrow ‘marker’ into any image. We call this network with the decoder attached the **color-picker**. We can then test whether an illusory configuration impacts performance of the color picker by placing a white arrow marker at several points of the illusory image and check whether the output is biased in a human-like fashion. This is the approach we use in the Lightness Contrast Effect and Adelson Checker Shadow Illusion.

### A.2.7 Lightness Contrast effects

**Psychological Significance:** In the Lightness Contrast effects our perception of two identical central gray patches is altered by their surround, such that a patch surrounded by a dark background is perceived as lighter, and the patch surrounded by a light background is perceived as darker. The standard explanation of this is that lightness perception is the product of the relative brightness of surfaces across a boundary given that this ratio will remain constant regardless of the general illumination, allowing lightness (and color) constancy. However, in the lightness contrast context, the mechanism designed to produce lightness constancy results in the central grey squares being perceived differently. These computations are thought to occur in the primary visual cortex [106]. Some DNNs can achieve color constancy [107] and other forms of constancy [54] under some conditions, although there remain questions as to whether this is achieved in a human-like manner. There are also computational theories of the lightness contrast effect [108], but we are not aware of any demonstrations that DNNs support this effect.

**Dataset.** The dataset consists of the standard Lightness Contrast configuration: square within a uniform canvas of different grayscale values. The user can specify the grayscale value of the center square, which is kept fixed, while the value of the background is varied. Importantly, each sample is replicated many times with the white arrow marker placed at different locations in the canvas. A color picker network can then be queried for the grayscale value at different locations in order to measure whether the perceived value of the central square is affected by its surroundings.

### A.2.8 Adelson checker shadow illusion

**Psychological Significance:** In this classic illusion [52], two squares on a checkerboard are perceived to have different reflectance due to one being in shadow and the other in light, despite being the same brightness. This phenomenon is explained with the ability of the human brain to perceive reflectance of a surface as invariant under variation of brightness. In this illusion, the patches inside and outside the shadow reflect the same brightness, and accordingly, the visual system assumes the patch in the shadow must be lighter.

**Dataset.** This dataset simply consists of the Adelson Checker Shadow illusory image replicated many times, grayscaled, with a white arrow systematically placed at different locations of the canvas, covering the whole checkerboard. A color-picker network (that is a decoder trained to predict the value of a marked pixel, e.g. trained on the Grayscale shape dataset, see Appendix A.2.6) is queried at all locations. Critically, the color-picker will show illusory perception if the pixels in the two target patches are seen as two different colours. In particular the pixels of the unshaded patch should be seen as darker than the shaded patch by the network.

### A.2.9 Thatcher Illusion

In this illusion the eyes and mouth of upright faces are inverted to produce a grotesque image of a person. The distinction between a normal face and a distorted face is highly salient. However, when faces are upside down, the distortions are much less salient. This effect was originally reported on images of Margret Thatcher, thus the name of the illusion. This effect is sometimes claimed to be more dramatic for faces compared to other categories, lending support to the hypothesis that face processing is special [49]. Other researchers claim that similar effects are observed for other types of objects [50]. [39] demonstrated that CNNs trained to identify faces exhibit a Thatcher-like effect, though they did not

assess whether this effect extends to other object categories. The extent to which this effect is specific to faces or can be generalized to non-face objects remains a subject of debate [e.g., see 50, 109, 110]. To test DNN sensitivity to the Thatcher Effect for both faces and non-face dataset, we provide both a Thatcherized dataset of faces and a Thatcherized dataset of words (in which individual letters are rotated).

**Face Dataset.** We provide a small dataset of celebrity faces using a subset of CelebA<sup>3</sup>, but the user can specify any folder containing images of faces. Each image is resized according to parameters specified by the user and then reoriented into both an upright and a 180-degree inverted configuration. Furthermore, it is either 'Thatcherized' or remains unaltered. To 'Thatcherize' an image we compute landmarks of the eyes and mouth, compute the bounding rectangle for each, and rotate them around their centre of mass. Blurring on the edge is applied to minimize artefacts. To assess the susceptibility of DNNs to the Thatcher effect in faces, we propose a similarity judgment analysis. This involves comparing the perceived similarity between each upright face and its Thatcherized counterpart, as well as each inverted face with its Thatcherized version. To align with human perception, the latter comparison is expected to yield a higher similarity score than the former.

**Word Dataset.** We employ a collection of 1000 English words or artificially generated sequences of random letters. All entries are uniformly presented in uppercase, covering a range from 3 to 8 letters in length. Following [50], to simulate the Thatcher Effect for words, we rotate one or more letters by 180 degrees. To increase variability, each word is displayed in one of ten different fonts, with variable font sizes, and includes jitter for each letter. The configurable parameters include the number of words, the exact or range of letter counts per word, the number or range of letters to be rotated, the font size, the level of jitter, and whether to use random strings or English words.

### A.3 Shape and object recognition

A key feature of human vision is that we identify objects largely based on their shape. For example, we can easily identify line drawings of objects with no colour and texture [111]. To measure shape bias in DNNs there is now a benchmark that tests models on "style transfer" images composed of the shape of one category and the texture of another [112]. Many DNNs, including DNNs that perform at the top of the leaderboard on Brain-Score, rely primarily on non-shape features, as they classify the images based on their texture rather than shape. More recent DNNs trained on much larger datasets have started to show a more human-like shape bias [113], but there are many additional attributes of human shape perception that need to be accounted for by any DNN model of human vision.

#### A.3.1 Identifying line drawings, dotted line drawings, silhouettes, and image segments

**Psychological Significance:** Humans can often identify line drawings of objects as quickly and accurately as photographs, highlighting the importance of shape for object identification [111]. Interestingly, a child who had never previously been exposed to line drawings can readily identify them, showing that there is no need to be trained on line drawings to identify them [58]. By contrast, DNNs need to be trained on line drawings in order to recognize them at human levels [60]. Similarly, humans can easily identify silhouettes of objects, whereas DNNs again struggle [although interestingly, they do better with silhouettes compared to line drawings; 61].

In addition, by exploiting the Gestalt principle of good continuation, humans can recognise line drawings with modified local features when the global shape is left intact. In our experiments, we modified line drawings in three ways: by replacing the continuous line with dots; by replacing continuous lines with segments; and by texturizing them. These images are easily identifiable, and accordingly, DNNs should be able to identify these out-of-distribution images.

**Line drawings dataset.** We use the line-drawing stimuli from [61], consisting of 36 classes from ImageNet (one line-drawing per class). The line-drawings are white stroke on a uniform canvas (black by default). We used this dataset to build the **Dotted line drawings and Image Segments datasets**. In the former case, the user can specify the dot size and the distance between dots. In the latter case, we have generated complementary images that have complementary segments removed (see Figure A.9). That is, each line segment in one image is absent in the other, and together the image is complete. These stimuli are generated by overlapping a grid on the line drawing and deleting complementary sections. The user can specify the grid orientation, the distance between each grid row and column, and thickness of each cell. Participants find these images trivial to identify, and accordingly, DNNs should also. Importantly, humans find complementary images like these hard to distinguish, and indeed, complementary images produce equivalent priming to repeated images, highlighting how the visual system treats them as equivalent [31]. This would also be the case if complementary dots were removed for the dotted line drawings. Thus a second approach to compare humans to DNNs is through a similarity judgment analysis across complementary images, which should return very high similarity value in some hidden layers of DNN.

<sup>3</sup><https://mmlab.ie.cuhk.edu.hk/projects/CelebA.html>

There are many datasets of line drawings available, and the user can specify any folder containing line drawings, to generate a dotted/segmented dataset. The line drawings are expected to be composed of a black stroke on a white background, but can otherwise be of any shape, and the line drawing folder is expected to contain sub-folders for each class (e.g. ‘airplane’) which can contain multiple line drawing instances for that class (this follows the standard structure used in many deep learning libraries for image classification, e.g. the ImageFolder dataset in PyTorch). Our script will automatically convert the image to a white stroke over a uniform background (black by default).

**Silhouette dataset.** For the Silhouette dataset, we use samples from [62]; 9 classes from ImageNet, each containing 40 samples. As before, the user can specify any folder containing silhouettes. Alternatively, the user can also specify a folder containing line-drawings (following the same constraints as above), which will be converted into silhouettes. Again, humans find these images easy to identify, so models should as well.

### A.3.2 Identifying familiar and unfamiliar images defined by texture boundaries

**Psychological Significance:** The human visual system can group elements in scenes based on texture, with texture regions defined by the similarity of their elements. This is an example of a Gestalt principle (Similarity) contributing to object recognition [114]. One way this manifests is through the ability to identify familiar (**texturized objects**) and perceive unfamiliar (**texturized unfamiliar**) by their texture.

**Datasets: Familiar and Unfamiliar Texturized Objects.** We provide a dataset of familiar texturized objects by using line drawings from [61] as base items. For unfamiliar shapes, we generated silhouettes of blob-like objects. For the pre-generated datasets, the texturization consists of masking the internal contour of a line drawing/silhouette with a pattern of a repeated character with a randomized font size, rotated by a random degree. The character is randomly selected from letters, digits, or punctuation, and we kept the background uniformly colored. When generating images, the user can also specify the texturization of the background as well, although we have found that doing so will turn object recognition from trivial to challenging, depending on the selected character.

The same approach is used for the unfamiliar shapes. In this case, the user can specify the number of blobs to generate and texturize. For both familiar and unfamiliar datasets, the user can specify how many texturization samples to generate for each input image.

To measure alignment with human visual perception, the different datasets require a different approach. For familiar shapes, DNNs can be tested by simply assessing classification accuracy. For unfamiliar shapes, a similarity analysis can be carried out. For example, a DNN should find a blob and its texturized counterpart more similar than a blob and a differently texturized blob (see example in Figure D.1).

### A.3.3 Identifying Embedded Shapes

**Psychological Significance:** The Embedded Figures Test [EFT, 64] is a widely utilized tool in research exploring individual differences in perception, with a particular emphasis on studies of autism spectrum disorder, and as a measure of local versus global perceptual style [115]. Subsequently, [64] developed a set of stimuli in which several Gestalt grouping principles were manipulated in order to create increasingly difficult matching to sample tasks. They found that the principle of good continuation (operationalized in terms of the number of continued lines from the original shape) impacted performance the most. Each target shape was integrated into four distinct contexts, each exhibiting a progressive increase in the number of lines extending from the target shape into its surroundings. The higher the number of lines extending the shape, the lower the performance, highlighting human susceptibility to camouflage and the role of Gestalt organisation principles in camouflage.

**Dataset.** We used the dataset from [64] who developed simple stimuli in which background lines camouflaged geometric shapes to various extent (Figure A.10). Importantly, different embeddings have different levels of continued lines from the original shape, which strongly affects human performance. Furthermore, we developed our version by generating 5 irregular polygons, embedding them in a set of lines, some random and some extending directly from the polygon’s edges (similarly to the original dataset). Many camouflaging samples can then be procedurally generated from each polygon. Training decoders to classify the simple geometric forms provides one way to assess the impact of embedding shapes on DNNs. Decoders would be trained on simple shapes (either our irregular polygons or the original shapes from 64) and would then be tested on the embedded version. A DNN with a human-like perceptual system should show reduced ability to identify the shapes, with the level of impairment being a function of the amount of lines originating from the polygon [as in 64]. Notice in this case, human alignment requires a degradation of performance after image alteration.

### A.3.4 Sensitivity to Global Shapes

**Psychological Significance:** Human object recognition relies more heavily on global shape representations than on local features, whereas there is evidence that DNNs rely more heavily on local features [61], even when trained to have a shape bias [62]. In [62], humans and DNNs were presented with silhouette stimuli in their normal format, fragmented, or in a ‘Frankenstein’ format where most of the local features are preserved but the overall configuration of the image was distorted. That is, the authors modified global shape while maintaining most of the local features. In particular, the ‘fragmented’ condition (see Figure A.11) divides the shape into two distinct, yet adjacent, entities while preserving the local characteristics of the object. The “Frankenstein” scenario involves adjusting the upper section back into alignment with the lower half, so that the bottom and top halves are mirror reversed. This method keeps the object intact as a single entity. Human performance was much reduced in both the Fragmented and Frankenstein conditions, but DNNs performed similarly in the Whole and Frankenstein conditions, highlighting the importance of the local features and the lack of weighting for more global features in driving their performance. Attempts to train networks to focus on the more global aspects of the images failed.

**Dataset.** We provide both the dataset extracted directly from [62] and a version in which the fragmented and Frankenstein versions are automatically generated from any silhouettes or line drawing samples. The [62] dataset contains 9 classes from ImageNet, each containing 40 samples. A network with visual capabilities aligned with a humans’ should suffer from performance degradation in both fragmented and Frankenstein condition, which can be measured through classification accuracy (as usual, with a network pretrained on ImageNet or some other image dataset).

### A.3.5 Invariance to Object Transformation

**Psychological Significance.** Humans possess the remarkable ability to recognize objects despite the different retinal images the objects project depending on changes in size, orientation, lighting, and placement [65]. This is performed on-line: an object, once seen in a new or altered form, can typically be recognized instantly in subsequent exposures at different angles, without further training. This capability applies irrespective of the object’s familiarity [66, 117]. Previous work [67, 68] found that none of the 7 tested classic visual DNNs possess on-line invariance architecturally (that is: training an object at a viewpoint would not automatically support object recognition at a different viewpoint, even for simple affine transformations such as translation). However, this ability could be induced by pre-training the model on the specific transformation of interest, and this would transfer to unfamiliar classes. For example, a network pretrained to classify images in which the objects are randomly rotated, develop on-line invariance to rotation, even for novel objects and novel classes. This partially extends even in transformation of viewpoint, in which the object is rotated in depth.

**Datasets: 2D Affine Transformations and Viewpoint Transformations.** We provide a separate dataset for affine transformations (rotation in picture plane, translation, scale, and shear) and viewpoint invariance (rotation in depth). The configurable parameters allow for a fine-grained analysis of the effect of each transformation. For each transformation dimension, the user can chose one or multiple ranges of training and testing. As in the previous datasets, the user can specify any folder containing line-drawings or silhouettes (or any image with a clear contour on a white background). For the viewpoint invariance dataset, we use the ETH-80 dataset [69]<sup>4</sup>, which contains 8 categories (apples, cars, cows, cups, dogs, horses, pears and tomatoes), each consisting of 10 object instances, and each object captured from 41 different viewpoints. For the pre-generated dataset, we avoided including views straight from the top. The configurable parameters allow the user to generated dataset only within a specific azimuth and inclination range.

For both the 2D transformation and viewpoint datasets, there are several ways to test whether a DNNs possess online invariance to transformation. First, a DNNs (not necessarily pretrained) could be trained on un-transformed images (e.g. with the object always in the center, unrotated, unscaled, or from a standard viewpoint). It could then be tested on various transformations of these objects. This could be used to establish whether the network is architecturally invariant to some transformations. Several pre-training steps could be used to test how the training environment affects performance. Another approach avoids training on the target classes (either because we want to test a pretrained network without altering its weights, or because we want to test the network on unfamiliar classes): a similarity judgments analysis is performed on transformed versions of the same object, and is compared to the similarity of different objects. A human-like DNN will have internal activations that are more similar for same objects across transformations, than for different objects. This is the approach used in [67, 68].

<sup>4</sup><https://github.com/chenchkx/ETH-80/tree/master>

### A.3.6 Same/Different Task

**Psychological Significance.** Human shape representations not only support object recognition but also a wide variety of additional functions, including visual reasoning. Perhaps the simplest form of visual reasoning is tested in the same/different task – judging whether two shapes are identical apart from their spatial location. Although DNNs can solve the same/different task when training and test images are highly similar to one another, performance drops when training/test images are dissimilar [70]. By contrast, humans can make same/different judgements for any visual patterns as long as they are perceptible.

**Same/Different Dataset.** The dataset was extracted from [70]. This dataset is composed of 10 conditions. Each image consists of two items placed randomly on the canvas. The two items can be either the same shape or a different shape and cannot overlap. Each condition consists of a different type of item used. By default, the items are composed of white strokes with no fill on a black background. See Figure A.12 for a summary of all the conditions.

The suggested testing methodology for this condition is slightly different than all other methods, and consists of training a DNN (not necessarily pre-trained) on a subset of conditions, and testing it on a different subset [as in 70].

## B Dataset Generation

### B.1 Pre-Generated Datasets

In the pre-generated dataset, we use 224x224 pixel images, and a variable number of samples depending on the task and condition (see section below on the number of samples). However, image size and dataset sizes are parameters that the user can easily modify if needed. The images in the datasets all have 3 channels (RGB). For almost all datasets, the user can specify the background color (either a uniform value, or request a different RGB value for every image), whether to use antialiasing, and the size of the item in the image relative to the whole canvas.

### B.2 Data Augmentation

We do not apply any affine transformation or other data augmentation techniques during the dataset generation phase. For instance, in the majority of Shape and Object Recognition datasets, a sample typically comprises a modified line drawing or silhouette centrally positioned on a canvas without rotation. We deliberately avoid creating replicas of the same sample with additional transformations. This approach prevents unnecessary expansion of the dataset’s size, as most popular deep learning libraries allow for an easy application of data augmentation. Furthermore, our testing methods allow for the application of affine transformation during testing through the configuration file, again avoiding the need to generate pre-augmented datasets.

### B.3 Number of Samples and procedural generations

Some datasets contain a fixed and limited number of samples. For example, the “NAP vs MP: line segments” dataset, recreating the stimuli used in [87], contains 3 conditions with 26 items each. This can be potentially expanded by changing the line stroke, the background color, or by applying dataset augmentation separately. For other datasets much larger samples with extremely low probability of repetition are easily constructed. For example, most Visual Illusions contain a “scrambled” condition in which the elements of the illusions are presented “scrambled up” on the canvas, with varying positions and orientation of each different element. A virtually limitless number of samples can be generated for these conditions, which is important since they are often used for training decoders. The pre-generated dataset typically includes approximately 5,000 samples for these conditions. For users requiring larger sample sizes, they can generate the dataset by changing the configuration argument relative to sample size (e.g., `num_samples_scrambled`) depending on their needs.

## C Models

We mainly focus on high-ranking BrainScore models. This criterion is a natural consequence of our motivation for MindSet. Within this framework we covered a variety of architectures, training schemes and model sizes. Thus, instead of just selecting the  $N$  highest ranked models we select a few from different architecture classes. All the models are taken from PyTorch Image Models (timm). We describe them here and provide links to the corresponding model cards.

1. **ResNet:** We use two models, ResNet-50 and ResNet-101, both trained on ImageNet 1k. These serve as “baselines” of sorts since they are the simplest models that are commonly tested on ImageNet. We test two variants, ResNet-50 and ResNet-101.

2. **ResNeXt**: These models are an extension of the vanilla ResNet: instead of using one feed-forward network within each residual block, they use multiple parallel paths which are aggregated at the end of the block. This was found to improve model performance. One important difference is that these models are not just trained on ImageNet: they are pre-trained on Instagram 1B. We test two versions with different size of the feature dimensions: a small version and larger version.
3. **ConvNeXt**: The evolution above naturally continues by applying the same idea to the convolution layer by using grouped filters. As with ResNeXt, these have better FLOP/accuracy ratio. They also achieve the best ranks in BrainScore, albeit by relying training on extremely large datasets, which raises the question of how much they have been trained on data like line drawings which human can correctly recognize without previous exposure. We test three versions of this architecture, including two of the highest ranked versions in BrainScore: a base model trained on LAION with data augmentation, a larger version trained on the same setup and an extra large version with no LAION pre-training or data-augmentation.
4. **ViT**: Shifting gears, we also test the basic Transformer architectures. Besides achieving a high rank in BrainScore, Transformers have become the most dominant architecture in neural networks and thus testing them is inherently interesting. We test three variants of ViTs: a a base one pretrained on CLIP, a larger patch version and a large-patch version that is pre-trained on LAION-2B. All models are fine-tuned on ImageNet-12K and then 1K.
5. **DeiT**: Much like the first three models, Data-Efficient Image Transformers (DeiT) are an extension of the standard Transformer incorporating several techniques that enable faster, more efficient training (such as better hyper-parameters and distillation). We test three versions of DeiT: a base-size version, a medium sized version, and a large version. The first two are trained directly on image ImageNet-1k, while the last one is pre-trained on ImageNet-22K and fine-tuned on the 1K version.
6. **FocalNet**: In a departure from the above, FocalNets are not tested on BrainScore. However, we find the idea behind them more interesting from a Cognitive Science perspective. In short, they replace the attention mechanism used in ViT to aggregate information across the image tokens (or patches) with a fovea-like mechanism. Said mechanism aggregates information across different scales around the patch, with larger scales trading of coverage of wider around the target patch for less resolution. This allows them to achieve competitive performance with ViT architectures while using less parameters. We test two variants: one with a small receptive field and one with a large receptive field.

## D Experimental design

Most of the tested datasets are set up as a simple experiment comparing two conditions, apart from classification tasks (though some datasets can be seen as conditions within an experiment - see below).

**Amodal completion** - in this dataset the similarity of two conditions (Occlusion and Notched) to a basis (No occlusion) are compared (see Figure A.1). Due to amodal completion, humans perceive the Occlusion condition as two overlapping objects. Therefore, the human-like result is higher similarity between Occlusion and the Basis (two separated objects) when compared to the similarity between Notched and Basis. We compared these similarities at each layer of each network.

**Relational vs Coordinate change** - in this dataset a change in the relationships between object parts is made or just a metric change where object parts change their position in coordinate space but retain the relations. The Relational change condition similarity with the Basis object should be lower when compared to the similarity between Coordinate change and Basis as humans are very sensitive to changes in relations between object parts but not to changes that preserve object part relations. We compared these similarities at each layer of each network.

**Metric properties vs Non-accidental properties** - in this dataset the Basis object can be changed in one of two ways: (a) a simple metric change (e.g., increasing the curvature of a curved object) or (b) a change in non-accidental properties (e.g., removing the curvature from the object altogether). As seen in examples from Figure A.1, changing non-accidental properties drastically changes how similar the object is perceived to the Basis. Therefore, the expected human-like result is that similarity between metric change (MP) and the Base object should be higher than between the non-accidental property change (NAP) and the Base. We compared these similarities at each layer of each network for three classes of objects (silhouettes, standard geons, and geons without shading).

**Decomposition** - in this dataset the Base condition has two shapes joined at one point of contact. One can split these objects into two objects naturally (at the point of contact) or unnaturally (by splitting one of the shapes). The Natural split, as the name implies, should be seen as more similar to the Base stimulus than the Unnatural split. We compared

these similarities at each layer of each network for two classes of stimuli; familiar stimuli where touching shapes are triangles, circles and other familiar shapes; unfamiliar stimuli made up of blobs.

**Depth drawings** - this dataset is slightly different as similarities are computed within conditions and then compared. Studies have shown humans easily find a target 3D shape among distractor shapes which are simply the target at a different orientation. However, when 2D features are extracted from the 3D shape and are used as targets, the search becomes harder. That is, it is more difficult to distinguish between targets and distractors even though the same transformation is applied to targets to create the distractors. Therefore, we computed similarities within each condition (3D shape, Inner features, All features). The expected human-like pattern is that similarity in the 3D shape condition is smaller than in both of the remaining two variants. We compared these similarities at each layer of each network.

**Ebbinghaus illusion** - in this dataset we trained decoders on outputs from each layer of each network to estimate the size of a red circle surrounded by randomly placed big and small white circles. Then, in the test phase, the decoders were required to estimate the size of red circles surrounded by big or small flanker circles. Humans perceive a target surrounded by large flankers as smaller than a target surrounded by small flankers. We computed the size estimate error as a percentage of the size of the stimulus presented. The human-like pattern would see overestimation of target size in the Small flanker condition and underestimation in the Big flanker condition.

**Müller-Lyer illusion** - the approach was similar to the one used in the Ebbinghaus illusion dataset. In this dataset, decoders were trained to estimate the length of the central shaft in the Müller-Lyer illusion. In the test condition, the line was surrounded by fins randomly placed on the canvas (and disconnected from the line). During testing, line length was estimated with Outward and Inward facing fins in the classical Müller-Lyer configuration. We computed the estimate errors in both conditions and compared them. The expected result is overestimation of line length in the Outward, and underestimation in the Inward condition.

**Jastrow illusion** - the experiment with this dataset follows the same logic as the previous two. Decoders are trained to estimate the size of curved shapes; during training, the shapes are disconnected and randomly placed on the canvas; during testing, the shapes are stacked perfectly on top of each other. Humans perceive the bottom shape as longer, although they are both the same size. We computed estimate errors for the top and bottom shape when both were of equal size. The expected human-like patterns is an overestimation of the bottom shape and correct or underestimation of the top shape.

**Shape recognition** - this dataset consists of 32 categories which the networks simply had to classify. The dataset is split into multiple conditions. Simple line drawings, dotted line drawing, silhouettes, and texturized shapes. In the texturized shapes we use either characters (e.g., "S", "\*", "@") or short line segments to create the texture. These shapes do not have explicit outlines. Shape recognition in these tasks requires synthesizing shape from various types of information. Humans have no issues recognizing objects in any of these conditions.

## D.1 Model assessment

We use three different measures to assess the models: Similarity Judgement, Classification/Regression and Decoders (Figure D.1):

1. **Similarity Judgement:** entails recording from the layers of interest (linear and convolution) for different inputs and comparing them according to the experiment in question. Such comparison can be performed with both cosine similarity or Euclidean distance, though for the tests presented here we exclusively use the former.
2. **Classification/Regression:** In this case we just register the output performance of the model. In general this may require training a new classification head if the number of output classes is different from the ones the model was trained on or the datasets have fundamental difference that are not relevant and may obfuscate the comparison. However, since we focus on different "stylizations" of the same ImageNet classes that models were trained on, this is not needed.
3. **Decoder Method:** For this method we attach linear probes to all the relevant layers in the model (linear and convolution) and train the decoder on some targets and test on others. Since we use this methods for illusions, we provide non-illusory conditions which the decoders are trained on. We can then test on the illusory conditions. Training is performed using Adam [118] with a learning rate of  $1e - 5$  over 20 epochs and batches of 100 examples.

## D.2 Analysis

The data analysis plan follows neatly from the experimental design. In the similarity-based methods we compute t-tests between described conditions, as well as effect size (Cohen’s  $d$  and  $R^2$ ) at each layer of each network. The exception are the three conditions in the **Depth drawings** experiments where there are three conditions and we compute a one-way ANOVA while reporting eta squared as the effect size measure. The same approach is taken for analyses of the three illusion effects based on the decoder method. Errors of estimate between conditions are compared using a t-test as described above. This is done for each layer of each network. The stimuli themselves serve as "participants" in these analyses, conducted at each layer of each network. Finally, there is no specific analysis for the classification performance in the shape recognition tasks.

## D.3 Other Testing Methods

The datasets featured in MindSet: Vision are suitable for a range of experimental approaches beyond the ones suggested in Section 3. For example, the relational reasoning capabilities needed to solve the Same/Different task could be tested by training a network (which does not need to be pre-trained) on one or a few of the ten available conditions in the Same/Different dataset, and then testing the network on the remaining conditions [as in 70]). In a similar vein, the 2D transformations and Viewpoint datasets could be approached by training a network on certain transformations/viewpoints and then testing it on the others, as demonstrated in [67].

Another efficient method to gain deeper insights into model performance is through ablation: by systematically removing or altering specific components of a neural network, researchers can evaluate the contribution of each specific layers, connections, or whole network components, providing a more nuanced understanding of the network’s functioning [119–121].

A further method that extends beyond our provided scripts is to input images into Multimodal Language-Vision Models and query them about what they see [23]. Assuming that the language output of these models provides a reliable window into its perceptual processes, this approach allows for an interactive examination of a model’s understanding of the images.

When GPT-4 first came out we tested it on some of our experimental conditions. We found that that it was proficient at recognizing silhouettes and line drawings, but struggled with textured representations of familiar objects. For example, a textured image of a banana was misidentified as either a crescent moon or a pair of scissors, and an airplane was mistaken for a butterfly. Moreover, we found instances in which GPT-4 is influenced from images it has previously processed, that is prior exposure to an image can lead the model to incorrectly identify later, differently textured images as the same as the initially viewed object. For instance, when the model is first presented with the silhouette of a banana, followed by a textured depiction of an airplane, it sometimes erroneously classifies the airplane as a banana (Figure D.2).

More recently, Tangtartharakul and Storrs [122] tested a range of multimodal models, including GPT-4o, on 22 of the 30 experiments included in the MindSet Vision Toolkit. They found that models did much better on the texture, dotted line, and silhouette images, but failed to match human performance on a wide range of low- and middle-level vision phenomena (they did not test the models on any of the illusions).

## E Results

In our statistical analyses we found that the vast majority of t-tests and ANOVAs were highly significant. Further, standardized effect size measures in those cases were almost uniformly indicative of large effects (some in the expected, human-like, direction and some in the opposite). Combined with the sheer number of comparisons made, there is little utility in attempting to present all the statistical analyses (all are available on our Open Science Framework repository). Instead, we will visualize all the findings across all layers of each network for similarity and decoder methods (means for each condition at each layer) as well as Top-1 and Top-5 classification performance from the shape recognition tasks.

This reveals two important points to take into account when interpreting results in studies which attempt to align deep network and human representations/neural activity/behavior. First, due to large numbers of stimuli/layers/parameters, degrees of freedom in statistical analyses get inflated and even minute differences may be associated with very small  $p$  values. Additionally, variance is usually much lower than in studies with human participants (if we had plotted confidence intervals for Figures E.1 to E.11 they would not have been visible). This can also lead to large standardized effect sizes. Neither the  $p$  values nor the standardized effect sizes by themselves provide enough evidence that an effect is similar to one found in human visual processing. Second, when analyzing network representations across many

layers, then picking the one layer where the effect is the largest is equally uninformative. We reported results using this approach in the main text as it will be familiar to the target community, but also because these largest effects, charitable to networks when in the expected direction, still cannot be described as human-like perceptual phenomena.

In the **Amodal** completion dataset (Figure E.1 most networks do show some evidence that Occlusion, compared to Notched stimuli, is represented as more similar to two intact objects when. One might conclude this is support for amodal completion in these networks. However, the magnitude of the effect is minimal and inconsistent across network layers. For networks such as `resnext101`, the difference is largest at early layers - which would be consistent with the explanation of the phenomenon arising in early-mid vision. However, it is then completely lost in the downstream representations. In other networks the difference is quite consistent throughout (e.g., `deit3_base`) but quite low in magnitude. The small magnitude of differences combined with high similarity of both conditions to the reference stimuli challenges the conclusion that the networks are producing a systematic effect of amodal completion.

Contrary to results from the Amodal completion dataset, in the **Relational vs Coordinate** change, networks seem to consistently represent Relational change as less drastic than Coordinate change (see early layers of `resnet50` in Figure E.2 as an example). Nevertheless, the findings do not provide much support for the conclusion that networks systematically treat relational changes as less important than coordinate changes: Similarities from the two conditions broadly match each other in magnitude and oscillations across network layers.

The most promising results using similarity-based measures come from the **Decomposition** dataset, particularly for unfamiliar shapes (See Figure E.7). We can see that for many of the networks the Natural split is represented as more similar to the Base stimuli (two shapes connected at a single point), than the Unnatural split (splitting the shapes by breaking apart one of them rather than at the point of contact). However, if this emerges in networks as it does with humans, there is a question as to why this effect is much smaller with familiar shapes. For example, in layers of the `convnext_xlarge`, the difference between similarities in the Natural and Unnatural conditions for the familiar shapes is at least 0.1, and the average difference is 0.125. By contrast, the average difference for the unfamiliar shapes is 0.212. This highlights the need for systematic experimentation to better understand how stimuli are represented in deep networks (rather than only show an effect in one set of stimuli without any experimental control or manipulation). Each of the datasets in MindSet lends itself to extensive experimentation and these results just provide a possible starting point.

The most problematic results from similarity-based measures come from the **Depth drawings** dataset. While humans distinguish between different orientations of features that are perceived as 3D shapes easier than they do for features perceived as 2D, the networks do not (Figure E.8). Indeed, although results are inconsistent across layers, some architectures, such as the `resnext101` networks, mostly follow the opposite pattern to humans. These findings suggest that 3D information is not being encoded.

Results from training decoders on layer outputs to test for whether illusory effects arise in the **Ebbinghaus**, **Müller-Lyer** and **Jastrow** illusions support several inferences. First, in most cases, the decoders are not able to generalize from training to test stimuli. This is reflected in the large estimate of errors in many cases (Figures E.9-E.11). This suggests that our decoder methods require further examination as the issues may have arisen due to the simplicity of the decoders or insufficient training. The most reasonable estimates for the **Ebbinghaus** illusion come from `resnet50` and the `resnext101` networks (Figure E.9). The smaller of the two `resnext101` networks differentiates between the Big and Small flanker conditions the best (at late layers). However, it is in the opposite direction of the one expected; the size of central circles surrounded by big flankers is overestimated, and the size of circles surrounded by small flankers is underestimated. Not to mention that the estimate errors are implausibly (compared to human perception) large at those layers. Results for the **Müller-Lyer** illusion are qualitatively different but equally unreasonable. `Deit3` and `VIT` networks produce the most reasonable estimate errors and, at some layers, a reasonable replication of the pattern we would expect (Figure E.10). Particularly `deit3_large` produces overestimation of central shaft lengths with outward facing and underestimation of lengths for shafts with inward facing fins in the middle layers. All of the mentioned networks also produce a steep increase of estimate errors in both conditions (and both in the direction of underestimating length) at the final layer. **Jastrow illusion** results again show that the magnitude of estimate errors is most reasonable in `resnext101` networks but there is no evidence of a systematic illusory or any other effect in any of the networks (Figure E.11).

Finally, results from **Shape recognition** tasks based on classification of ImageNet categories reveal that networks struggle on all five classes of stimuli (Figure E.12). Models do best in the simple line drawings and silhouette conditions, but still, performance is much worse than humans (well over 90% on average). The gap increases further in the remaining conditions while human performance remains above 90% (see the BrainScore competition and the BMD2024 behavioral benchmark).

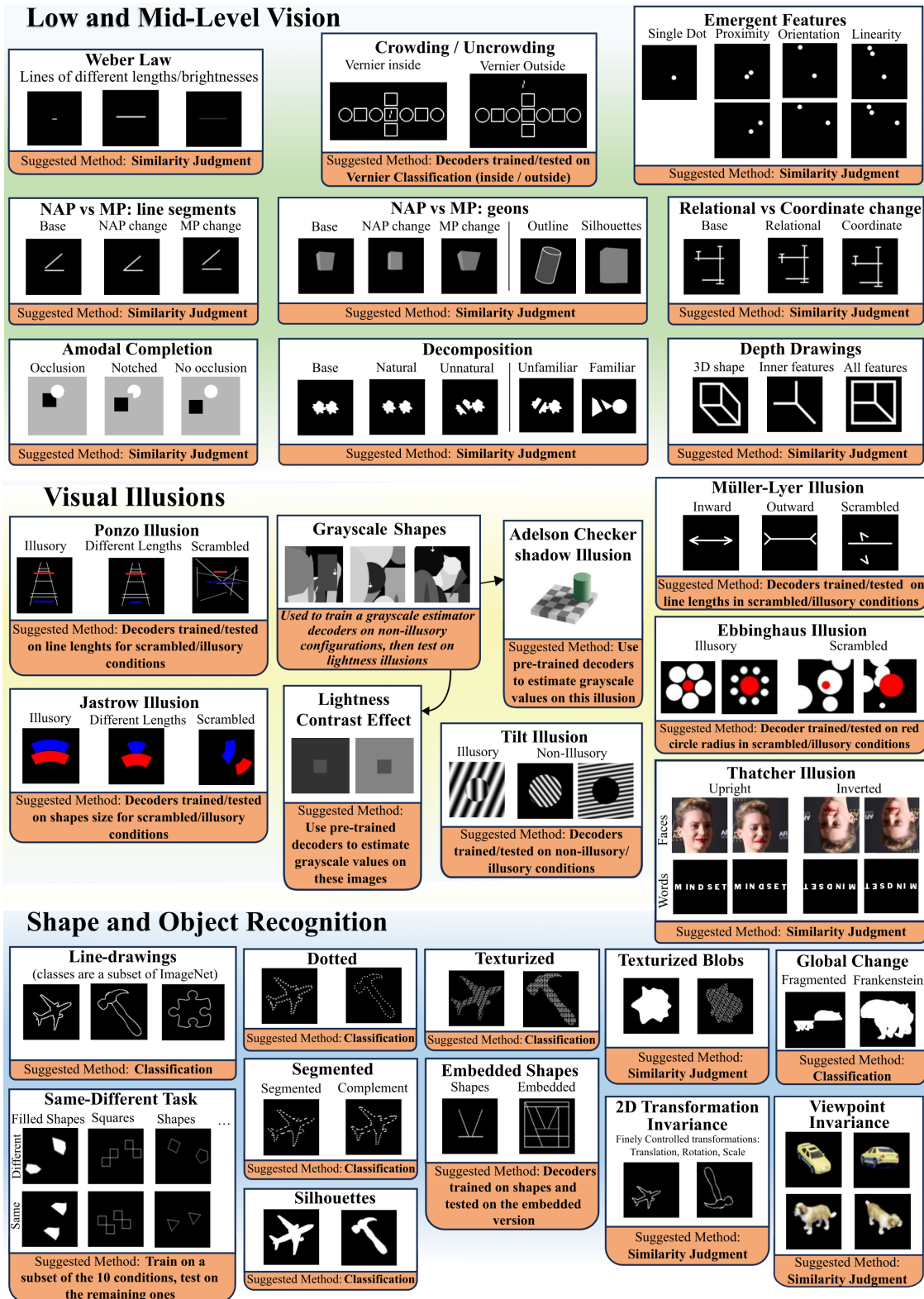


Figure A.1: Comprehensive overview of the ‘MindSet: Vision’ datasets, arranged in three main categories. Each panel represents a distinct dataset, which is further divided into conditions. The images provide examples from these conditions, generated with default parameters. We also include the suggested way to perform the comparison in each case. These are the ones used for the datasets that we test.

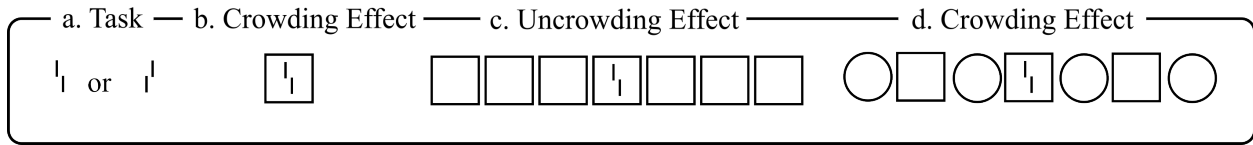


Figure A.2: Illustration of the Crowding and Uncrowding effect. a. Observers perform a vernier discrimination task. A standard approach consists of measuring the vernier offset for which observers correctly discriminate in 75% of the trials. With the vernier alone, the offset is quite small. b. When a square is added the performance drastically drops (that is, the threshold-offset increases). This is the classic crowding effect. c. Adding more flankers increases performance again. This is referred to as uncrowding. d. The magnitude of crowding and uncrowding effects is contingent upon both short-range and long-range spatial interactions between visual elements. Furthermore, the specific characteristics and spatial positioning of flanker stimuli play a crucial role in modulating these effects. For example, the performance drops again for the depicted pattern.

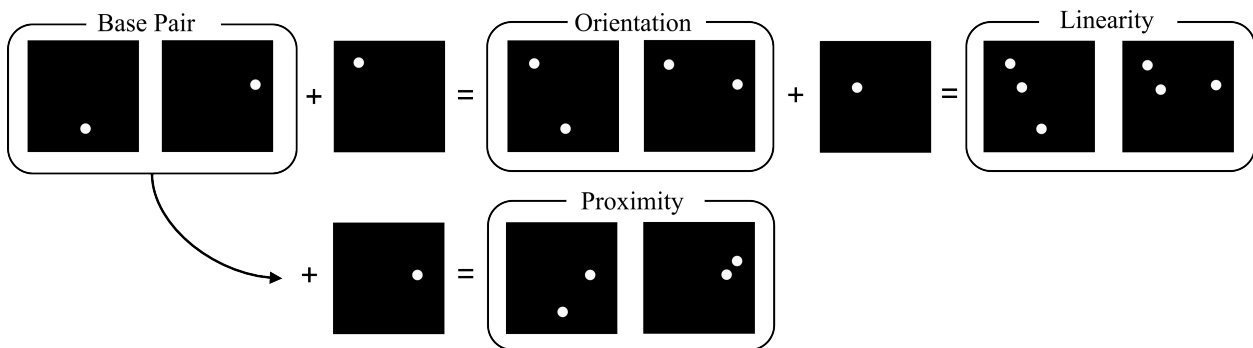


Figure A.3: Schematic of the generation procedure for producing a set of dotted stimuli. Starting with a pair of images in which the only discriminant feature is the location of a dot (Base Pair), an additional dot is added, yielding the Emergent Feature of proximity or orientation. The Emergent Feature of linearity is obtained by adding a dot to the orientation pair. Notice that the added dot is the same to both elements of the pair so it does not add on its own any discriminative features, but it generates additional features in relation with the surrounding dots.

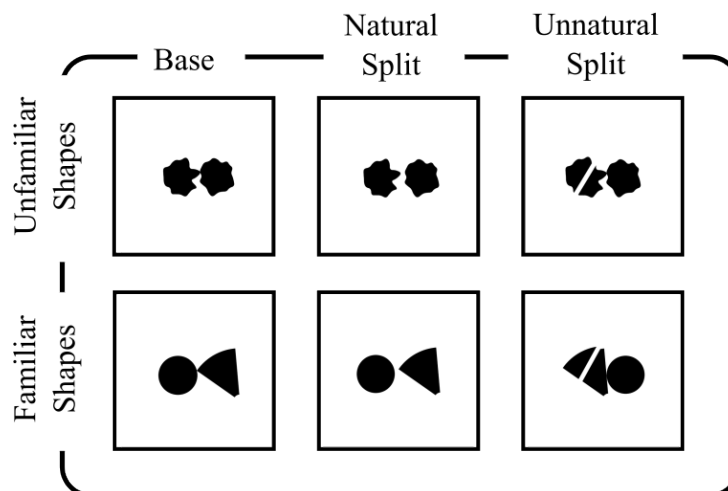


Figure A.4: The dataset features base images depicting two objects in contact at a single point. It includes two variations: natural and unnatural splits. In natural splits, the objects are separated, while in unnatural splits, the division occurs within an object itself. Identifying differences between base images and unnatural splits is simpler than distinguishing between base and natural splits. The dataset presents examples with both familiar and unfamiliar shapes, showcasing the diversity in object recognition challenges.

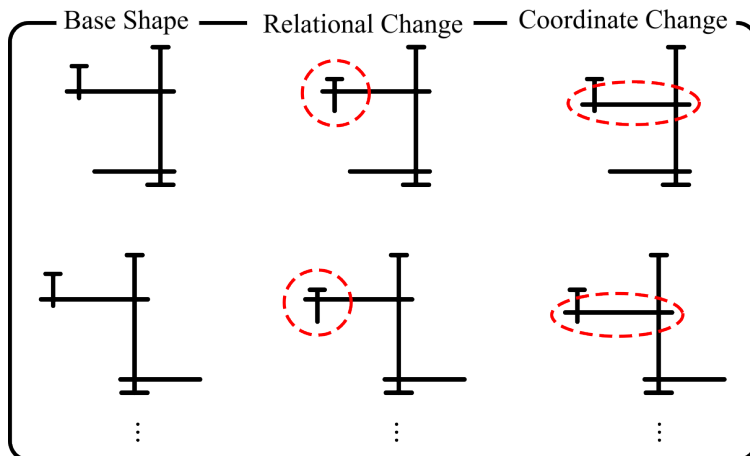


Figure A.5: Reproduction of stimuli used in [36]. Starting with a base shape, the Relational Change variant was created by moving one part of the base object up or down (red dashed circle). The move was chosen to change the categorical above/below relation between the circled part and the part to which it is attached. The coordinate change variant was created by moving the whole horizontal (red circled) segment up or down, together with the part moved in the relational change. This resulted in no categorical relations change. Therefore, the perceived difference between a base and its relational-change pair is greater than the perceived difference between the corresponding base-coordinate change pair.

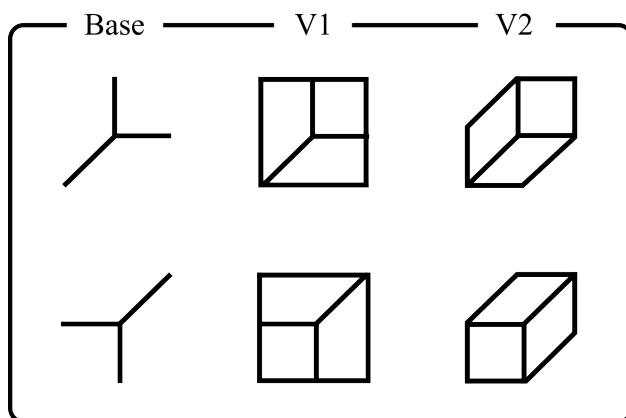


Figure A.6: Illustration of the 3D Drawing dataset stimuli. One where segmented lines (Base shapes) are augmented with contextual features to clearly form distinguishable 3D shapes (V2), and another where the additions do not contribute as strongly to depth perception, making shape discrimination challenging (V1). Importantly, the identical contextual features applied to each pair highlight that enhanced discrimination stems solely from the perceived depth, rather than the features themselves.

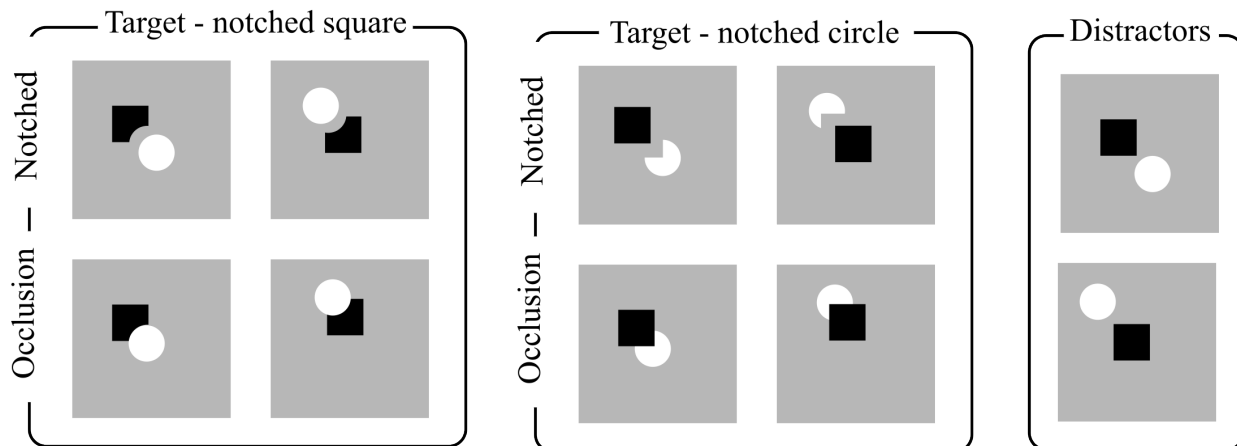


Figure A.7: Illustration of the Occluded Shape stimuli as used in [38]. The experiment compares three conditions: a baseline condition with squares and disks with no occlusion, an occlusion condition in which one object obscures part of the other, and a notched condition in which the occluded part of the object in occlusion condition is removed. This turns the notch into a distinctive feature and effectively creates a differently perceived shape despite the visible parts being the same as in the occlusion condition. The finding that notched circles and squares are more easily identified than occluded circles and squares is taken to reflect amodal completion.

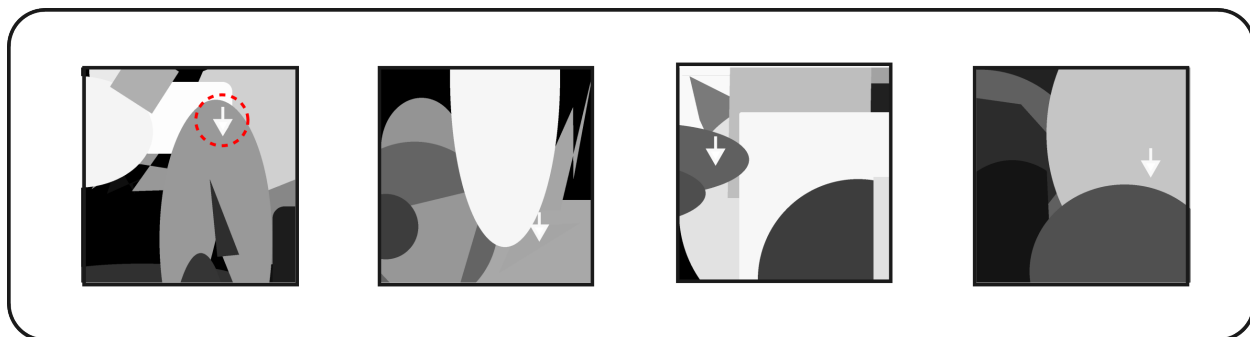


Figure A.8: Samples of five images from the grayscale dataset, used to train a color-picker, as detailed in the text.

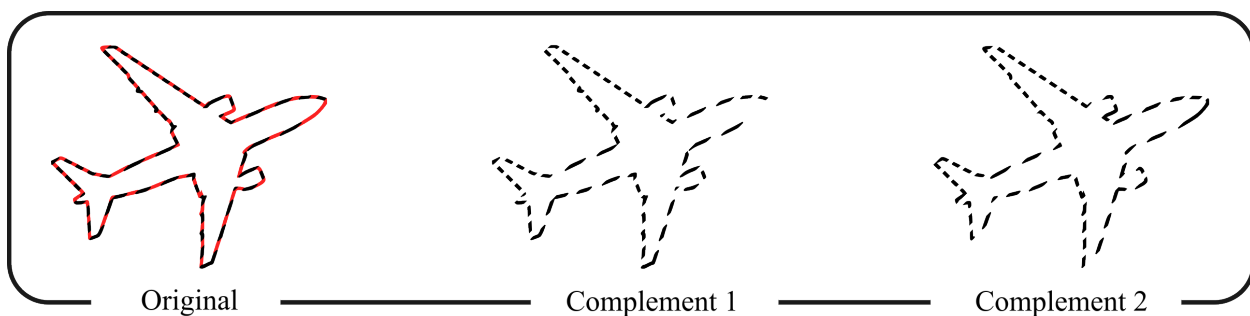


Figure A.9: Example of the complementary segment dataset. Each linedrawing results in two images with complementary segments removed. The resulting samples are very difficult to discriminate for humans [31].

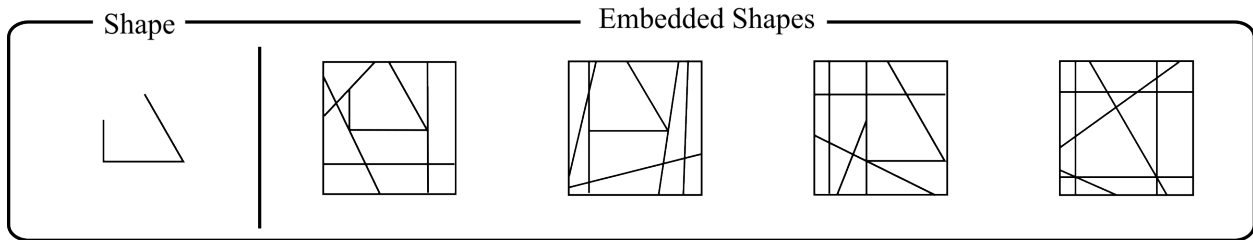


Figure A.10: Illustration of one set of items from the embedded shape dataset. These are the stimuli recreated based on [116]. A basic shape is camouflaged using a variety of horizontal and vertical line, and extending the segments composing the shape. We also provide a variation of this dataset in which, given a set of polygons, camouflaged versions are procedurally generated.

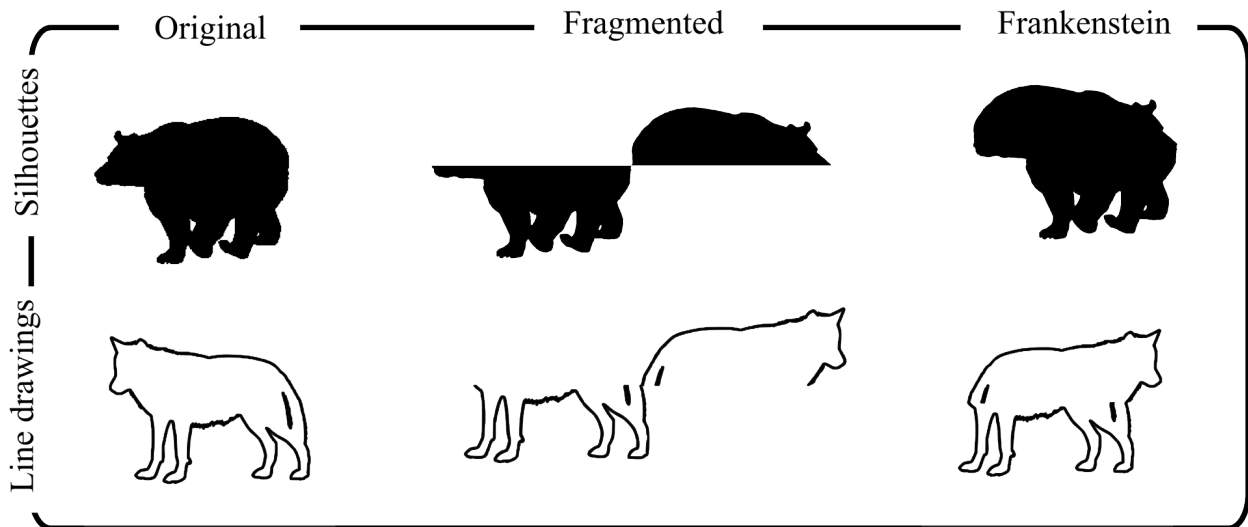


Figure A.11: Example of a stimulus and its transformed version, following [62].

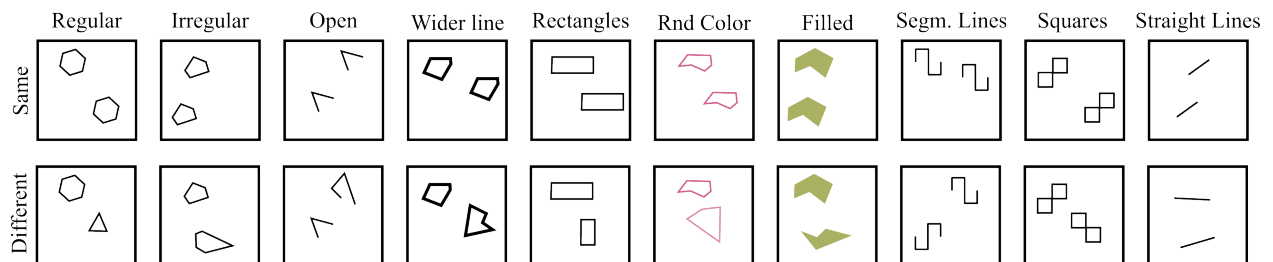


Figure A.12: Illustration of the ten conditions used for the Same/Different task. Two items can be either the same or different shapes up to translation. For the ‘straight lines’ condition, the “same/different” dimension considered is the line orientation (with length kept fixed).

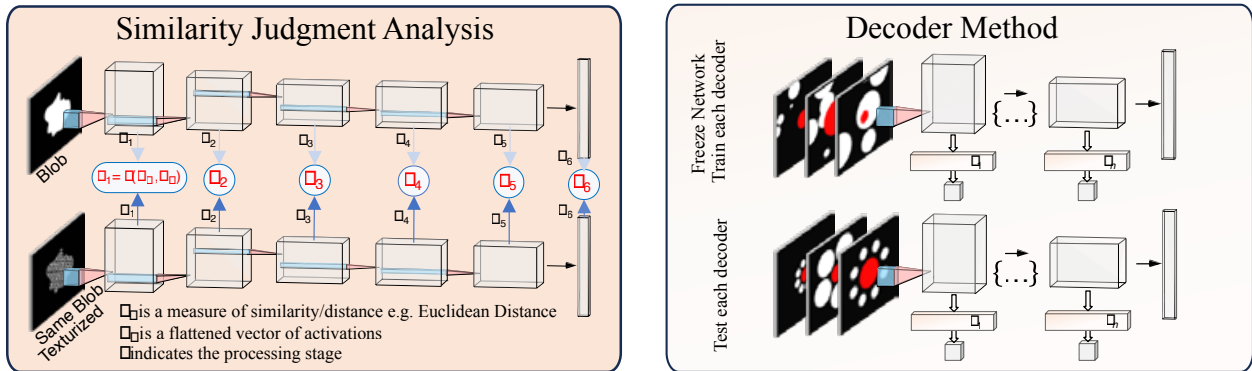


Figure D.1: The Similarity Judgment Analysis (left panel) involves feeding pairs of images to DNNs and comparing the elicited internal representations. We illustrate this method via the ‘Texturized Unfamiliar’ dataset composed of white and texturized blobs. The Decoder Method (right panel) involves training and testing a simple linear layer attached to different stages of a frozen network. In the given example, we assess the response to the Ebbinghaus illusion. Evidence that a DNN is processing images like humans would be that the decoder outputs larger estimates of red circle sizes when surrounded by smaller compared to larger white circles.

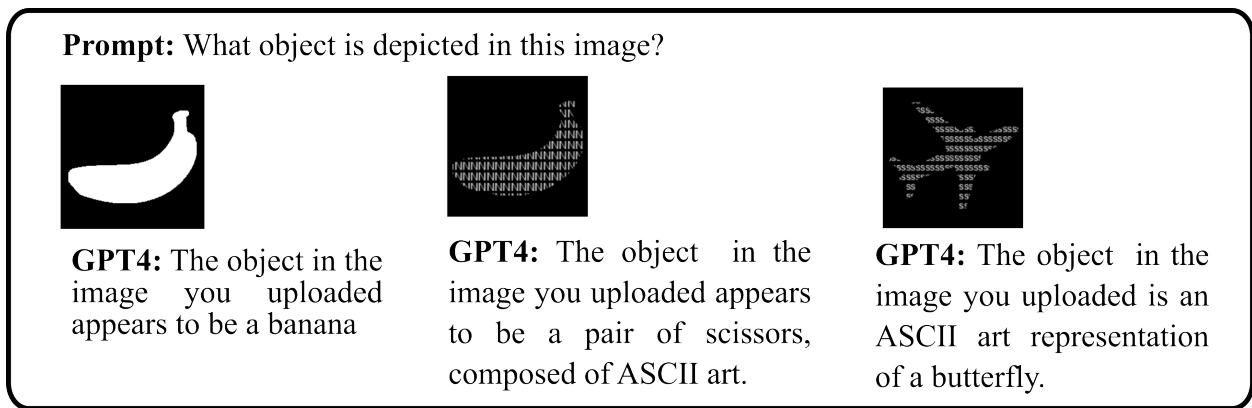


Figure D.2: Another way to test vision-language models is to simply ask them what they see. Here are samples of GPT4 responses after being prompted by different images from our silhouettes and texturized datasets, each time spawning a new conversation. The model accuracy drops significantly with texturized images. Interestingly, GPT4o does better. More testing on the various experiments in MindSet would provide evidence as to whether this reflects better ANN-human alignment or simply more training, including training on images similar to these test items.

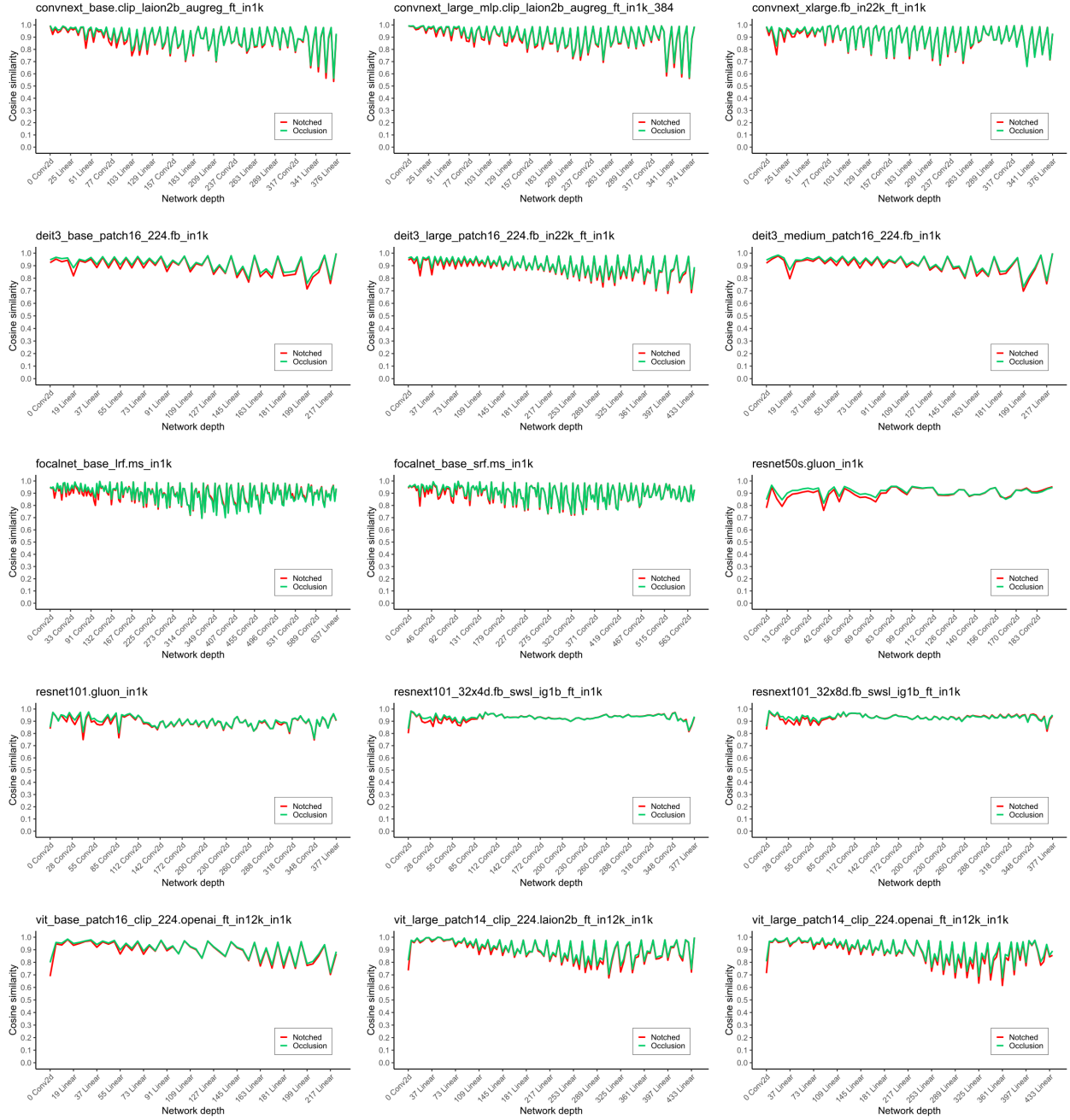


Figure E.1: Cosine similarity of the No Occlusion condition with the Notched and Occlusion conditions. If the networks exhibit amodal completion, we would expect similarities for the Occlusion condition to be significantly higher than in the Notched condition. The overall pattern of results suggest that networks do not manifest amodal completion as differences between the conditions are minimal. However, as noted in the main text, the layer with the largest effect does show a small effect in the right direction

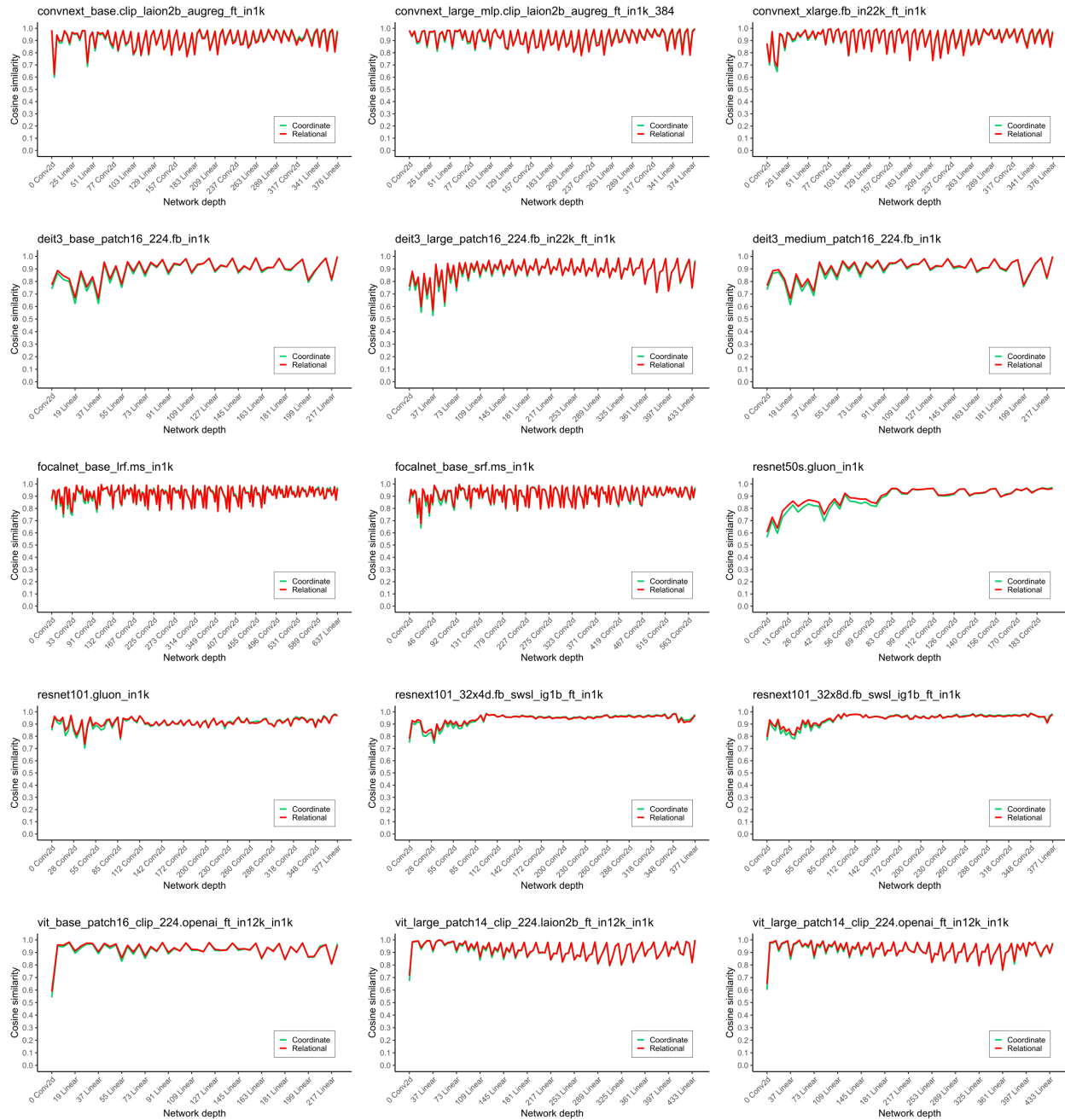


Figure E.2: Cosine similarity of the Base condition with Relational and Coordinate change conditions. Humans quickly and easily distinguish between a Base object and the corresponding Relational change object. On the other hand, humans are poor at noticing small metric changes where object parts are moved in coordinate space but relations between object parts are preserved. If networks "experience" the same phenomenon, we would expect similarities in the Coordinate condition to be much higher than those in the Relational condition. This is not the case, results very much overlap.

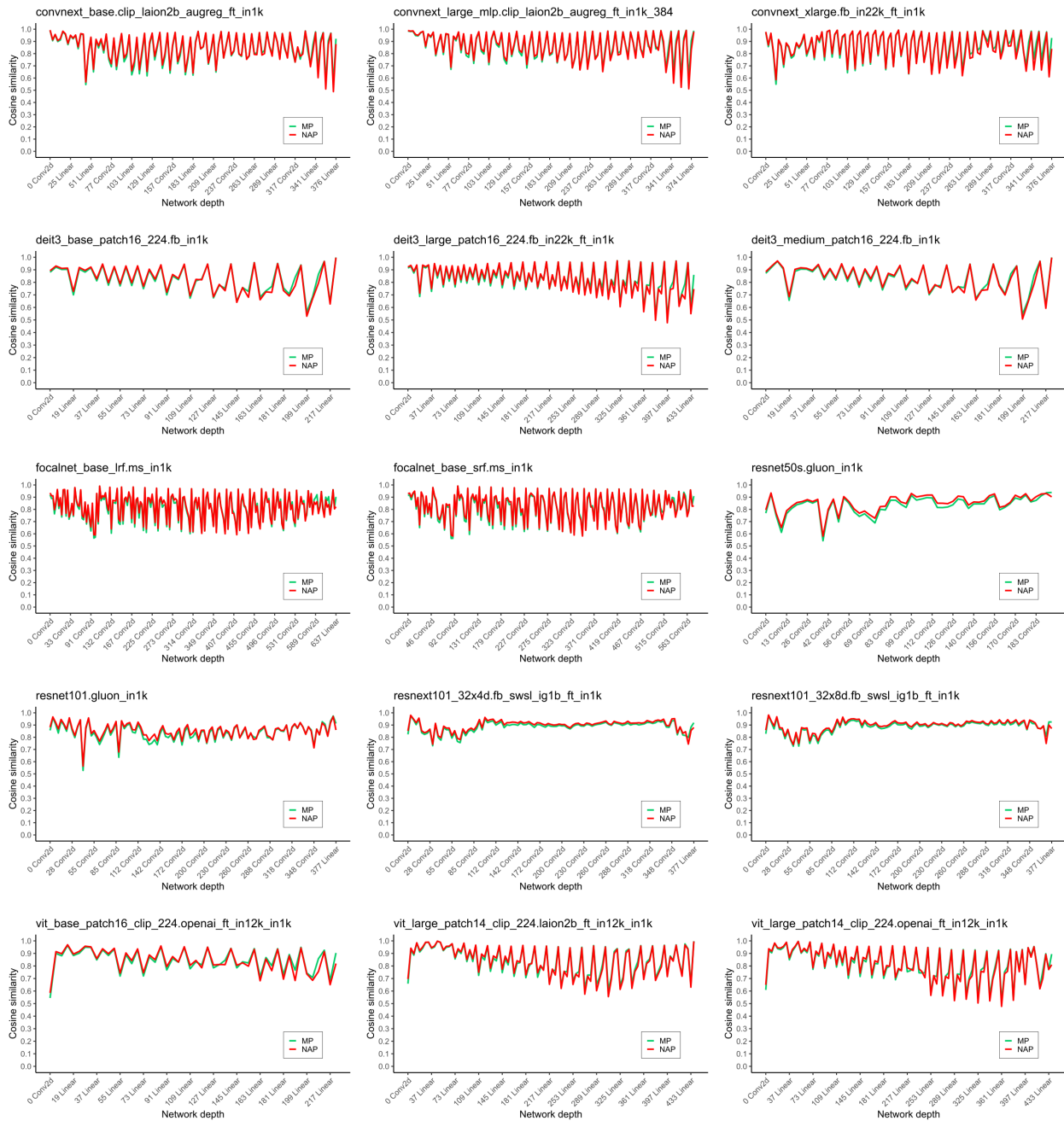


Figure E.3: Cosine similarity of the Base condition with a metric property change (MP) and with a non-accidental property change (NAP) to the Base stimuli for Silhouettes. Humans are very sensitive to NAP changes and to match this similarity in the MP condition should be much higher than in the NAP condition. This is not the case, as results vary very much overlap. But gain, as noted in the main text, the layer with the largest effect does show a small effect in the right direction

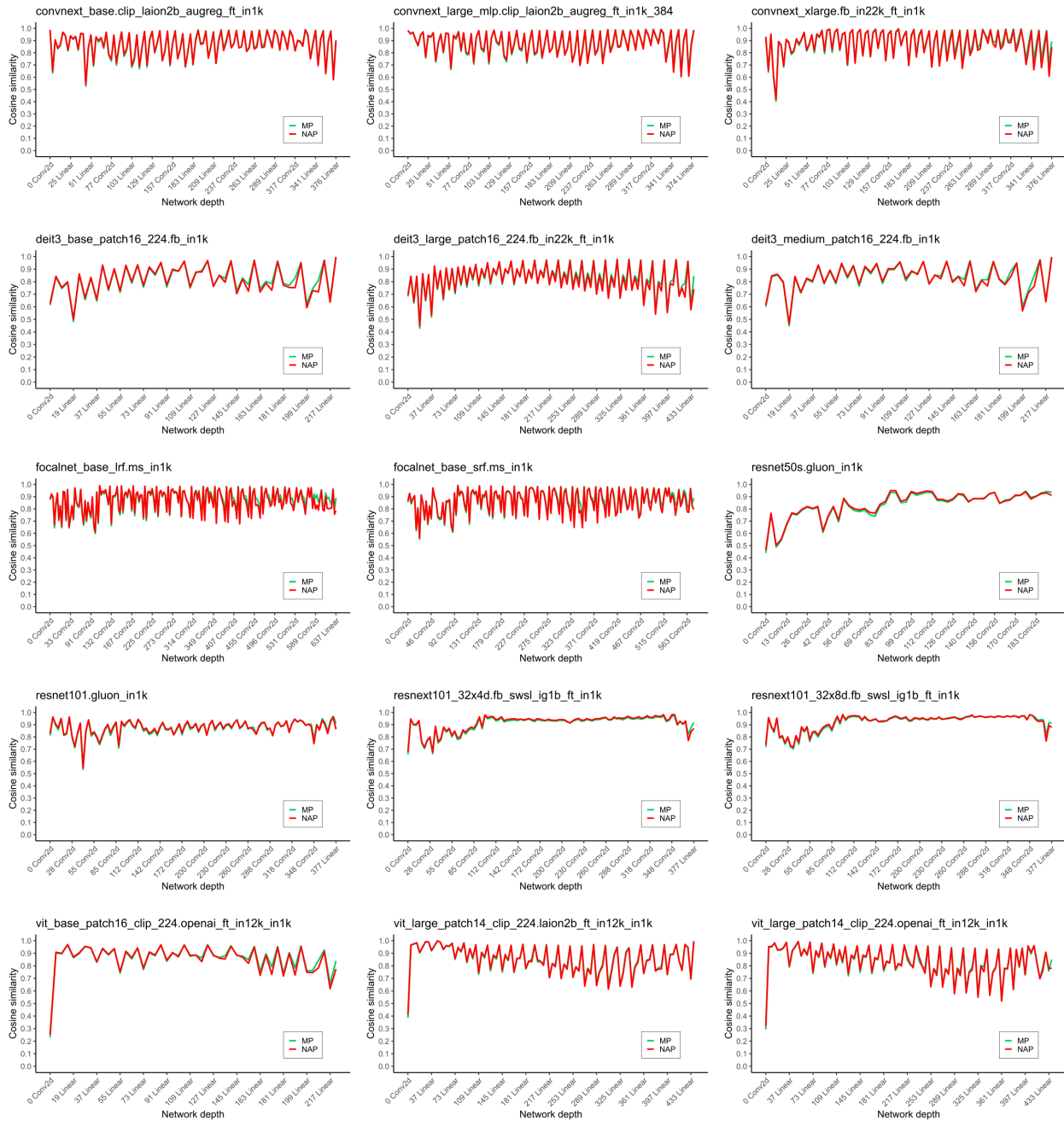


Figure E.4: Cosine similarity of the Base condition with a metric property change (MP) and with a non-accidental property change (NAP) to the Base stimuli for Geons with no shadows. Humans are very sensitive to NAP changes and to match this similarity in the MP condition should be much higher than in the NAP condition. This is not the case, results very much overlap.

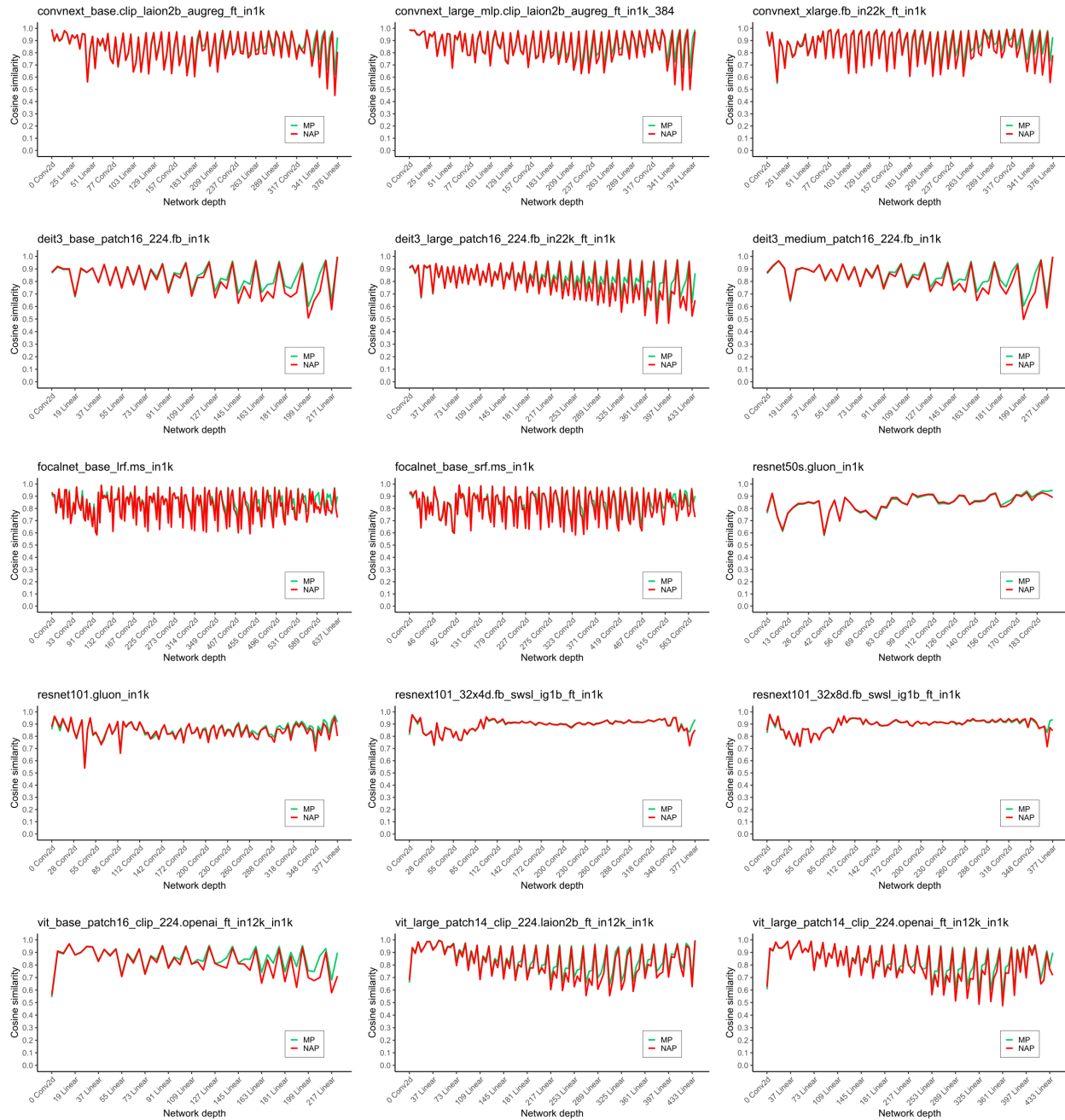


Figure E.5: Cosine similarity of the Base condition with a metric property change (MP) and with a non-accidental property change (NAP) to the Base stimuli for Standard Geons. Humans are very sensitive to NAP changes and to match this similarity in the MP condition should be much higher than in the NAP condition. This is not the case, results very much overlap.

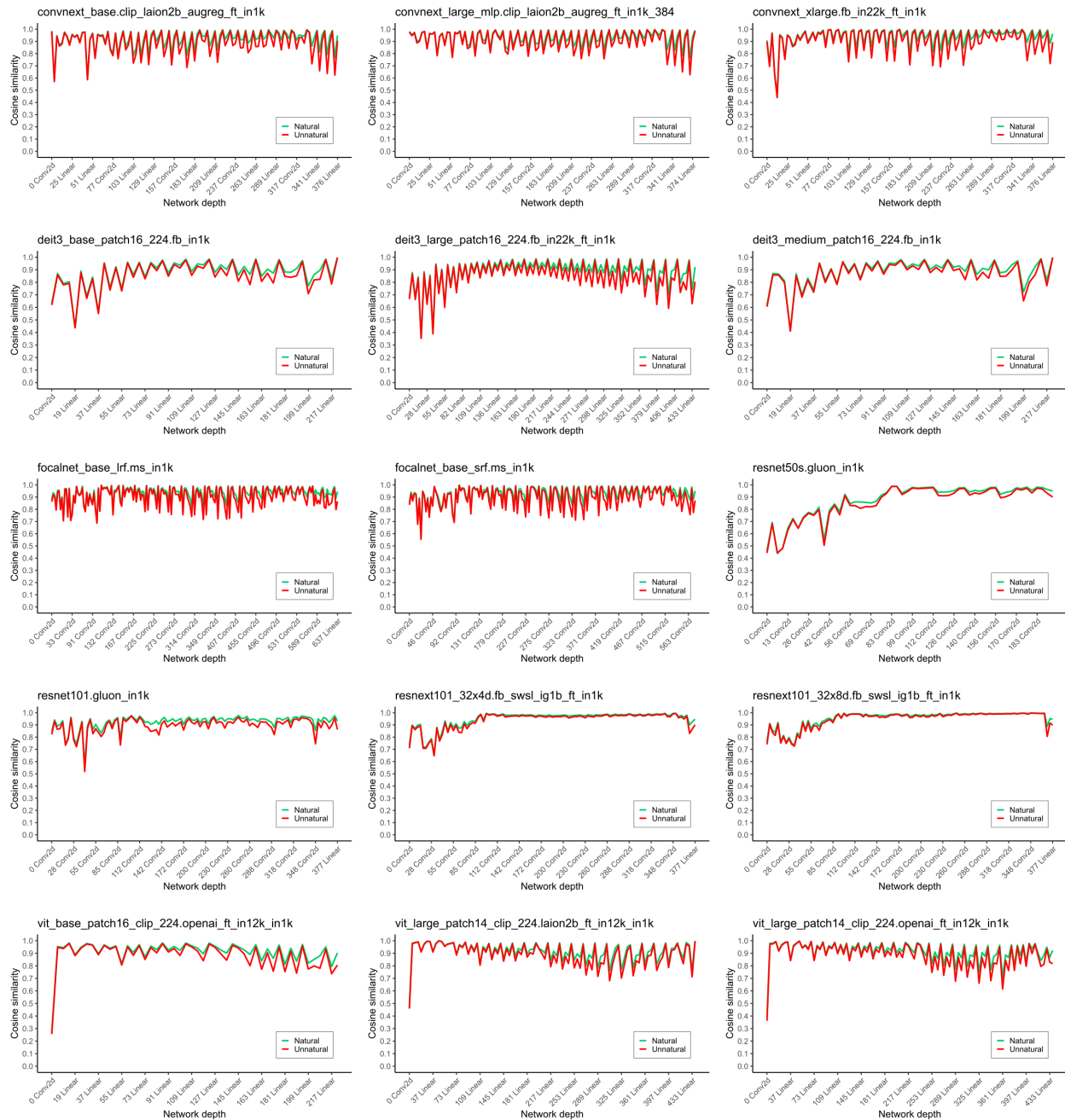


Figure E.6: Cosine similarity of the Base condition (two shapes touching) to Natural and Unnatural splits in the Familiar shapes stimuli. The human-like pattern of results would see the similarity in the Natural condition be higher than in the Unnatural condition. Some of the networks do exhibit this pattern at different depths, but the difference is far from decisive.

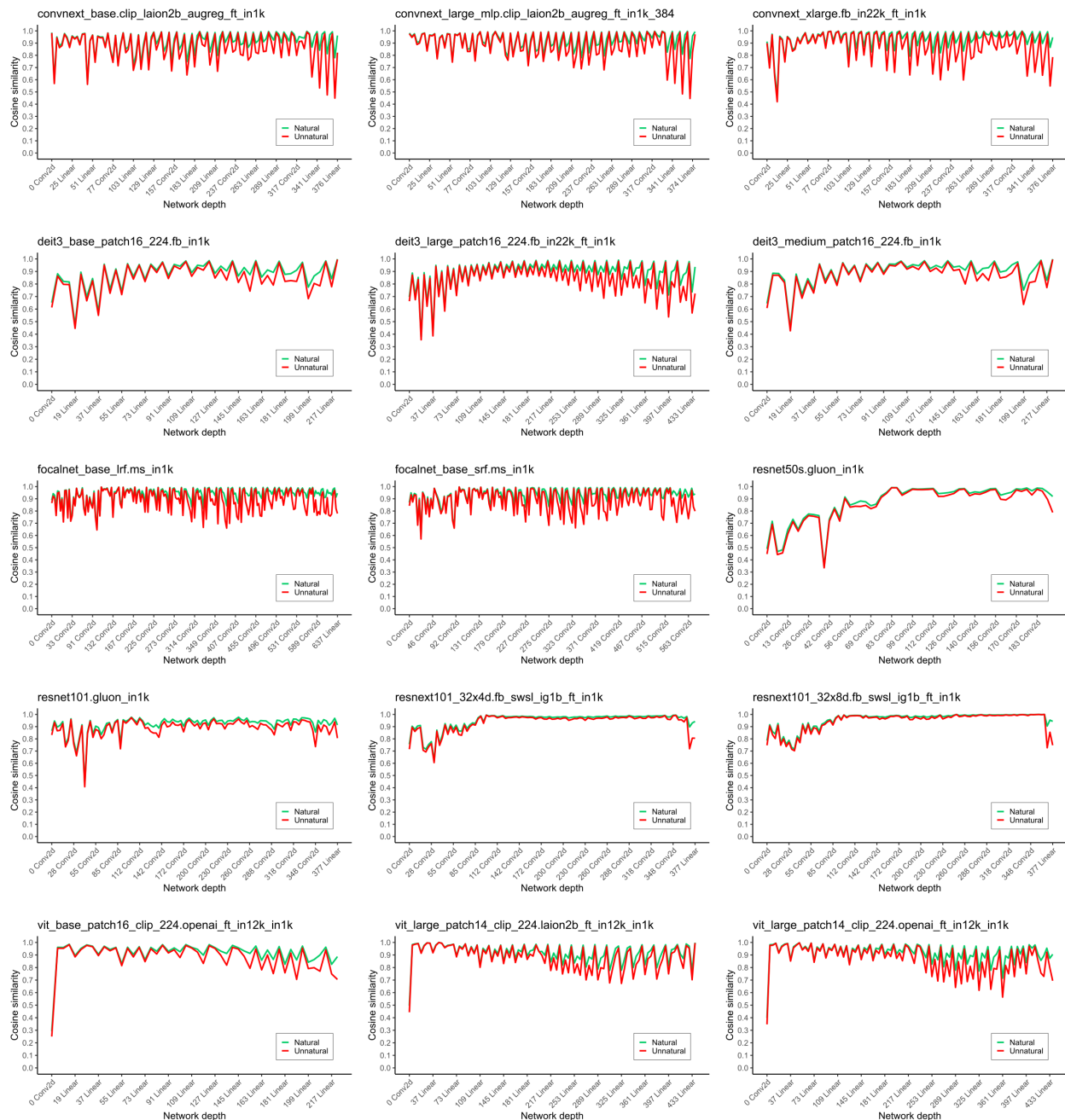


Figure E.7: Cosine similarity of the Base condition (two shapes touching) to Natural and Unnatural splits in the Unfamiliar shapes stimuli. The human-like pattern of results would see the similarity in the Natural condition be higher than in the Unnatural condition. Some of the networks do exhibit this pattern at different depths, but the difference is far from decisive.

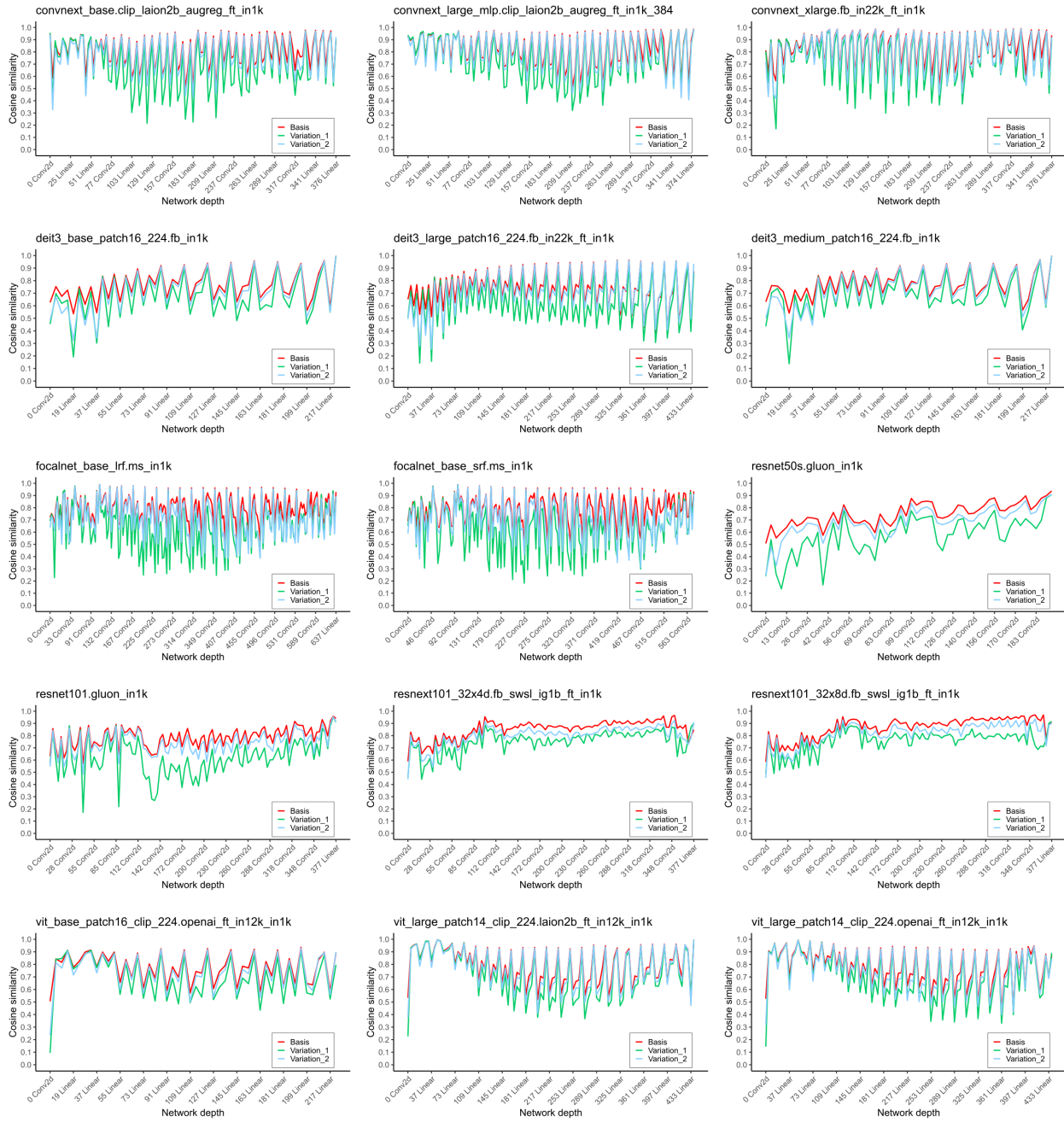


Figure E.8: Cosine similarity between differently oriented objects within each condition of the Depth drawings dataset. Humans find it easier to distinguish a 3D object from the same object in a different orientation than they do with stimuli made up of 2D features. Therefore, it would be expected that similarities in the Basis condition (3D objects) are higher than in both Variation 1 (Inner features) and Variation 2 (all features) conditions. This is not the case. Results for some networks very much overlap and are in the opposite direction for others.

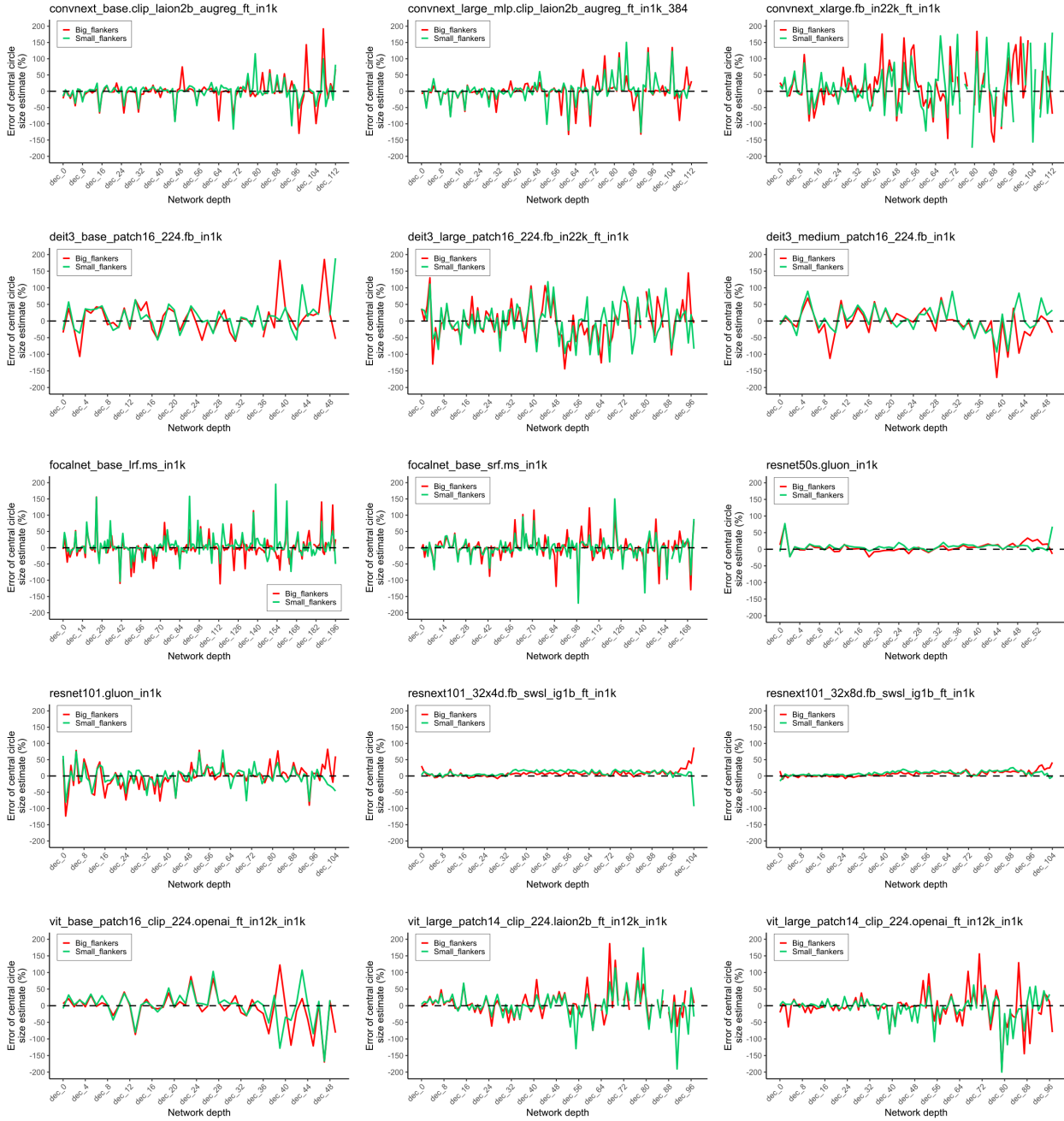


Figure E.9: Decoder errors of central circle size estimates in the Ebbinghaus illusion. Humans perceive the middle circle in the Ebbinghaus illusion as smaller when it is surrounded by bigger flankers and bigger when it is surrounded by smaller flankers. If this were the same for the networks, decoders trained on outputs from their layers would overestimate the size in the Small flanker condition and underestimate it in the Big flanker condition. Note that decoders generalize very poorly when trained on outputs of many networks, even making negative predictions (errors exceeding 100% below 0%). Results beyond the y-axis range have been truncated rather than increasing the range which would decrease clarity.

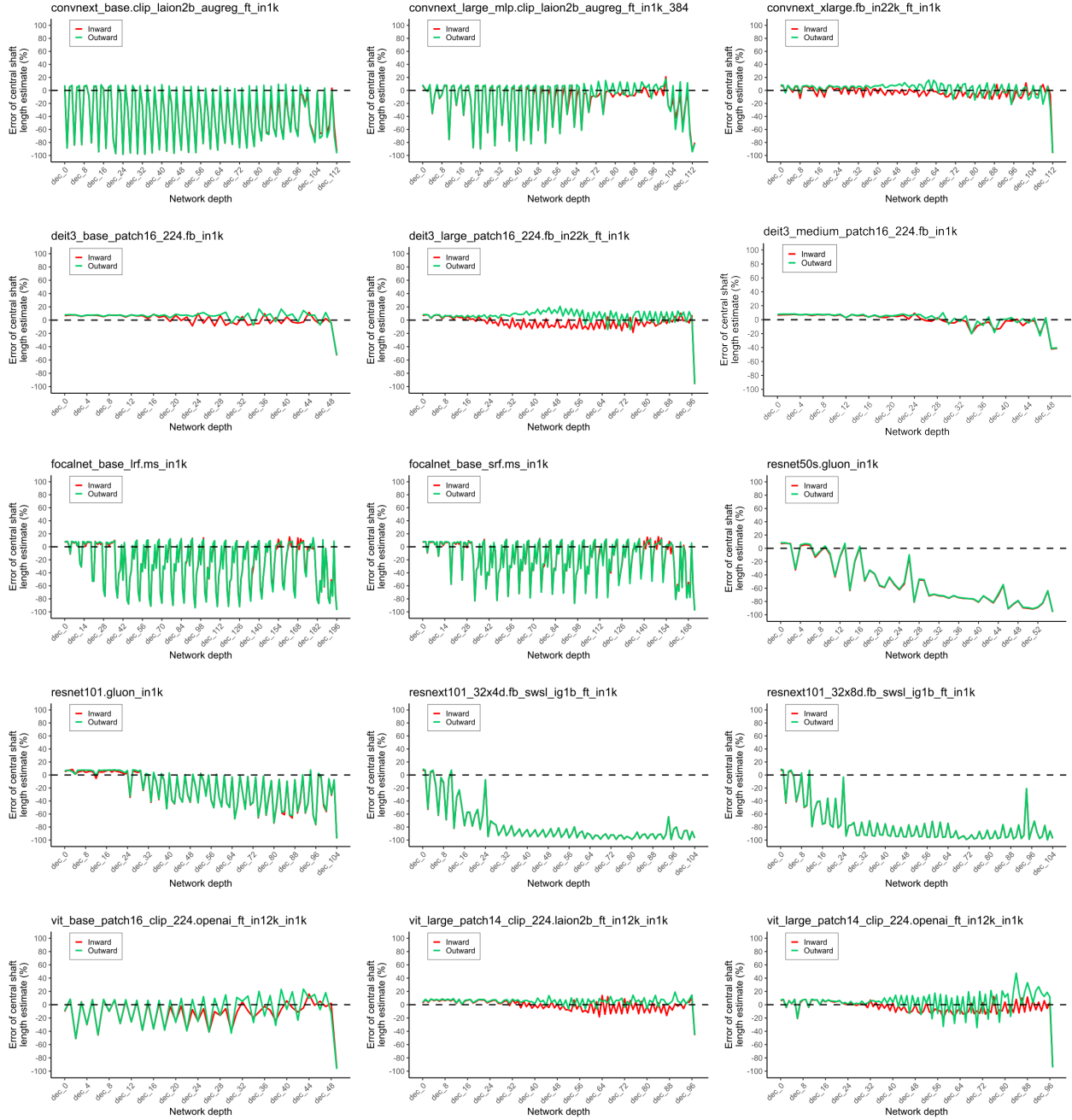


Figure E.10: Decoder errors of central shaft length estimates in the Müller-Lyer illusion. Humans perceive the central shaft as shorter when terminating with Inward facing fins, and longer when terminated with Outward facing fins in the Müller-Lyer illusion. If this were the same for the networks, decoders trained on outputs from their layers would overestimate the length in the Outward condition and underestimate it in the Inward condition. Decoders trained on some networks do exhibit this pattern of results at certain depth alongside reasonable estimates while other decoders provide very poor estimates overall.

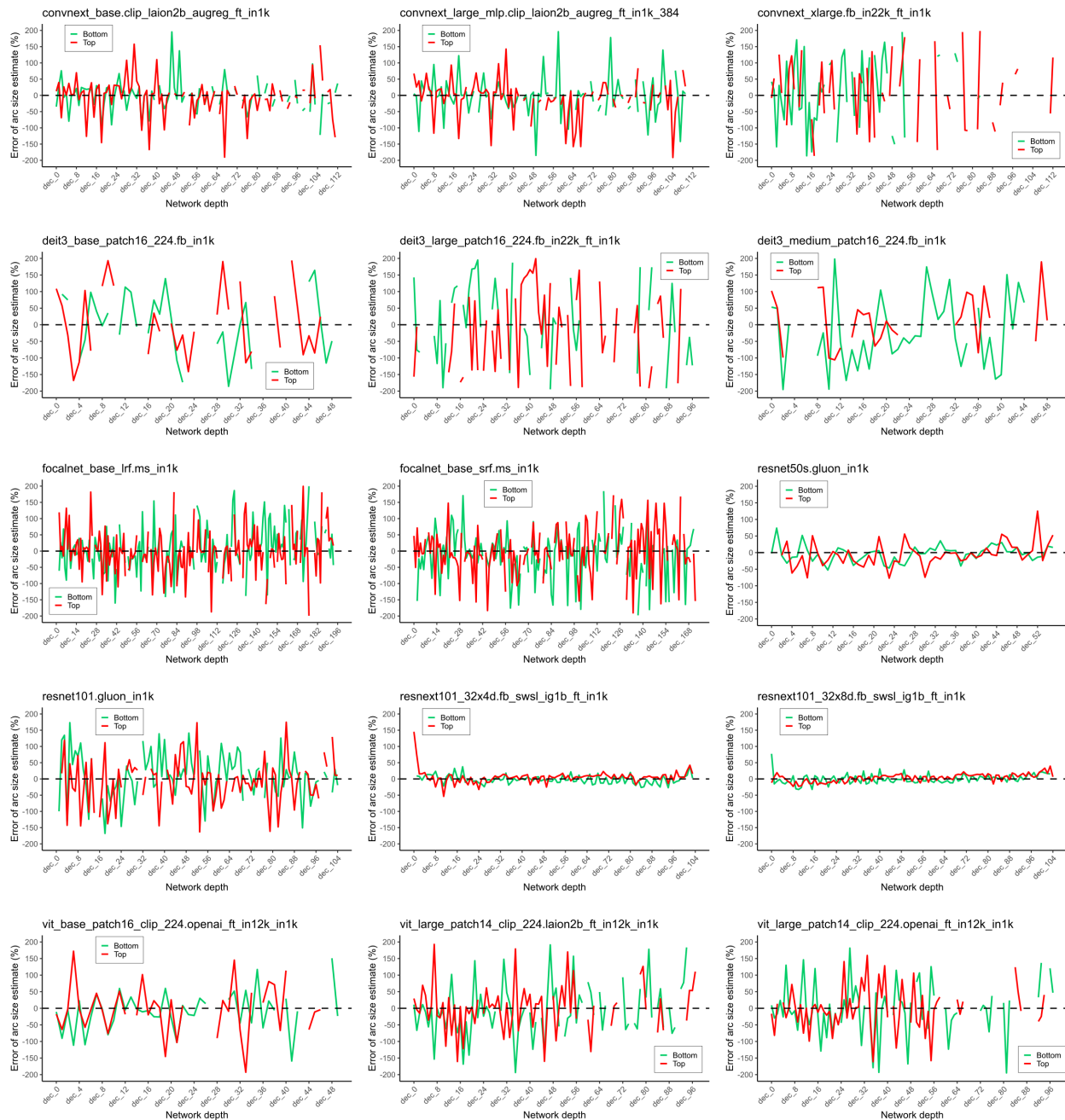


Figure E.11: Decoder errors of shape size estimates in the Jastrow illusion. In a configuration with two arced shapes of the same size stacked perfectly on top of each other, humans perceive the Bottom shape as longer than the Top shape. If this were the same for the networks, decoders trained on outputs from their layers would overestimate the size of the Bottom shape, and underestimate it for the Top shape. Note that decoders generalize very poorly when trained on outputs of many networks, even making negative predictions (errors exceeding 100% below 0%). Results beyond the y-axis range have been truncated rather than increasing the range which would decrease clarity.

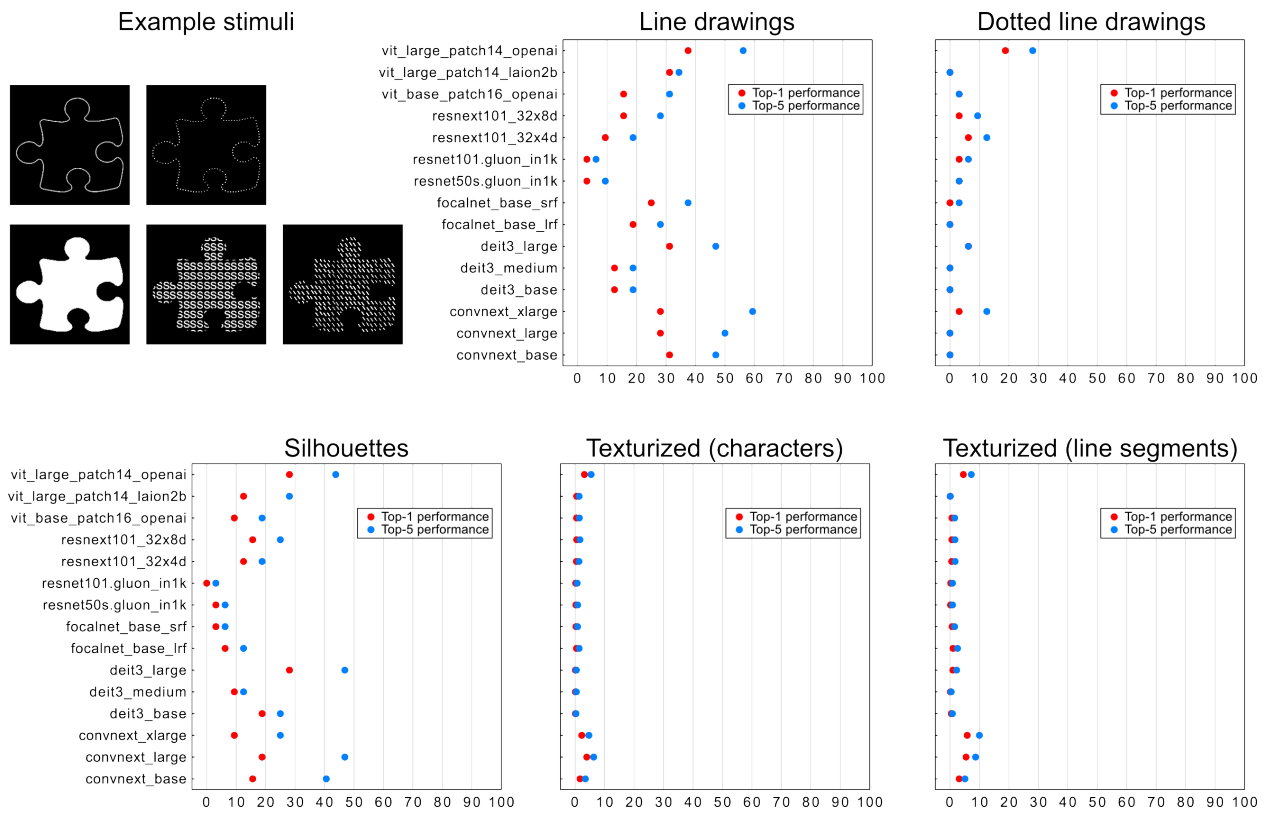


Figure E.12: Classification performance of networks for shape recognition. Note that when both Top-1 and Top-5 performance is 0%, only one dot appears in the figure.

## F Accessibility and Licensing

Pre-generated datasets are accessible for viewing and download on Kaggle in both a comprehensive version and a "lite" version, which can be found at large and "lite" respectively. Croissant metadata for both versions are automatically generated by Kaggle and can be downloaded from the Kaggle page. These datasets comprise a collection of folders containing .png images and associated metadata. Notably, each dataset's root folder includes a .csv file containing metadata for each individual image, as well as a .toml file detailing the configuration parameters used in dataset generation. This structure enables precise replication of each dataset published on Kaggle using our provided codebase. The dataset is made available under the CC 1.0 Universal license. The entire dataset generation process is tested on Windows Server 2022 (Windows 10/11), macOS 14.4.1, and Ubuntu 20.04. Authors assume full responsibility in the event of any rights violations.

The codebase for regenerating the dataset with varying parameters is hosted on GitHub, licensed under MIT. Comprehensive documentation on dataset generation procedures is included in the main README file within the repository. The code containing the experiments applied to each network is hosted on a different repository. While the original MindSet repository contains examples on how to run each experiment, the focus on modularity and code re-usability could be a source of confusion for researchers wanting to run their own custom experiments. The new repository on the other hand contains individual scripts with hard-coded values for each experiment. Thus they should serve as clear examples showing how the models are evaluated. Researchers can use these as a basis for running their own experiments with customized procedures. We provide ways to evaluate models with the three different methods outlined above. In the near future we will integrate both repositories for better accessibility.

The raw outputs of model evaluations, results of analyses, and scripts with accompanying documentation are hosted as a fully open Open Science Framework repository.